Perturbations in eIF3 subunit stoichiometry alter expression of ribosomal proteins and key components of the MAPK signaling pathway.

Anna Herrmannová[1#*], Jan Jelínek[2#], Klára Pospíšilová[1], Farkas Kerényi[1], Tomáš Vomastek[3], Kathleen Watt[4], Jan Brábek[5], Mahabub Pasha Mohammad[1], Susan Wagner[1], Ivan Topisirovic[6], and Leoš Shivaya Valášek[1*]

[1]Laboratory of Regulation of Gene Expression, Institute of Microbiology of the Czech Academy of Sciences, Prague, Videnska 1083, 142 20, the Czech Republic
[2]Laboratory of Bioinformatics, Institute of Microbiology of the Czech Academy of Sciences, Prague, Videnska 1083, 142 20, the Czech Republic
[3]Laboratory of Cell Signaling, Institute of Microbiology of the Czech Academy of Sciences, Prague, Videnska 1083, 142 20, the Czech Republic
[4] Science for Life Laboratory, Department of Oncology-Pathology, Karolinska Institutet, Solna, Sweden
[5]Laboratory of Cancer Cell Invasion, Faculty of Science, Charles University, Prague,
Vinicna 7, 128 43, Czech Republic
[6]Lady Davis Institute, Gerald Bronfman Department of Oncology, Department of Biochemistry, Division of Experimental Medicine, McGill University, Montréal, H3T 1E2, QC Canada

[#] These authors contributed equally to this work.

* To whom the correspondence should be addressed: herrmannova@seznam.cz
valasekl@biomed.cas.cz
Tel: +420 241 062 288
Fax: +420 241 062 665

Running title: eIF3 & signaling and stress transcripts

ABSTRACT

Protein synthesis plays a major role in homeostasis and when dysregulated leads to various pathologies including cancer. To this end, imbalanced expression of eukaryotic translation initiation factors (eIFs) is not only a consequence but also a driver of neoplastic growth. eIF3 is the largest, multi-subunit translation initiation complex with a modular assembly, where aberrant expression of one subunit generates only partially functional subcomplexes. To comprehensively study the effects of eIF3 remodeling, we contrasted the impact of eIF3d, eIF3e or eIF3h depletion on the translatome of HeLa cells using Ribo-seq. Depletion of eIF3d or eIF3e, but not eIF3h reduced the levels of multiple components of the MAPK signaling pathway. Surprisingly, however, depletion of all three eIF3 subunits increased MAPK pathway activity. Depletion of eIF3e and partially eIF3d also increased translation of TOP mRNAs that encode mainly ribosomal proteins and other components of the translational machinery. Moreover, alterations in eIF3 subunit stoichiometry were often associated with changes in translation of mRNAs containing short uORFs, as in the case of the proto-oncogene MDM2 and the transcription factor ATF4. Collectively, perturbations in eIF3 subunit stoichiometry exert specific effect on the translatome comprising signaling and stress-related transcripts with complex 5' UTRs that are implicated in homeostatic adaptation to stress and cancer.

Keywords: translation initiation; 40S subunit; eIF3; MAPK; ribosomal protein; differential expression; ribosome profiling

INTRODUCTION

Translational control contributes significantly to the overall regulation of gene expression. Indeed, regulation at the level of translation provides quicker adaptive and usually reversible responses to environmental cues than transcriptional regulation as it acts on pre-existing mRNAs by simply turning their expression on or off (Sonenberg and Hinnebusch, 2009). As such, translational control critically contributes to the maintenance of overall cellular homeostasis, suggesting that its dysregulation has detrimental effects on cell proliferation and, more broadly, on health (Scheper et al., 2007). In a rapidly growing number of cases, mutations and/or impaired expression of many translational components have been shown to either directly lead to or significantly contribute to various pathological conditions, including cancer (reviewed in (de la Parra et al., 2018b; Robichaud and Sonenberg, 2017; Spilka et al., 2013; Sriram et al., 2018)).

Translation can be divided into four stages with the initiation stage playing the most critical role with respect to translational control. It begins with the formation of the 43S pre-initiation complex (PIC) composed of the 40S ribosomal subunit, the eIF2*GTP*Met-$tRNA_i^{Met}$ ternary complex (eIF2-TC), and eIFs 1, 1A, 3, and 5 (reviewed in (Valášek, 2012)). The next step is the mRNA recruitment to form the 48S PIC, which is facilitated by the eIF4F cap-binding complex in concert with eIF3. Once the mRNA is loaded, the 48S PIC starts scanning the mRNA's 5' untranslated region (UTR) until the start codon has been recognized by base-pairing with the Met-$tRNA_i^{Met}$ anticodon. This drives conformational changes in the 48S PIC, co-operatively mediated by eIF1, eIF1A, eIF2, eIF3 and eIF5, resulting in the closure of the 40S mRNA binding channel and subsequent ejection of the eIF2*GDP*eIF5 subcomplex to allow subunit joining to commence (reviewed in (Hinnebusch, 2017)).

Cellular stresses primarily inhibit cap-dependent translation initiation *via* the eIF4F and eIF2-TC complexes. The former is under the control of two major stress-signaling hubs – the anabolic kinase – the mechanistic target of rapamycin complex 1 (mTORC1) and the mitogen-activated protein kinase (MAPK). They promote growth under nutrient-rich and stress-free conditions and deactivate in response to limited supply of amino acids, oxygen, ATP, growth factors or nutrients and play a role in the unfolded protein response (Bhat et al., 2015; Lindqvist et al., 2018; Roux and Topisirovic, 2018). These pathways are hyperactive in the vast majority of cancers, mainly due to activating mutations of RAS, BRAF and PI3K or loss-of-function mutations of the tumor suppressor PTEN, which are among the most common genetic perturbations in cancer (Kandoth et al., 2013). The latter – eIF2-TC – is a major target of the pro-survival, adaptive pathway called integrated stress response (ISR) encompassing four members of the eIF2α kinase family (PERK, PKR, GCN2 and HRI) that respond to a multitude of stimuli including nutrient limitation and endoplasmic reticulum stress by rapidly shutting down general translation (Pakos-Zebrucka et al., 2016).

Mitogen-activated protein kinase (MAPK) cascades have been shown to play a key role in the transduction of extracellular signals into cellular responses. Three families of MAPK signaling pathways have been well characterized in mammalian cells: extracellular signal-regulated kinase (ERK), c-Jun N-terminal kinase/stress-activated protein kinase (JNK/SAPK), and p38 kinase (Cargnello and Roux, 2011; Zhang and Liu, 2002). The activation of MAPKs is a multistep process. In case of the best described Raf-MEK-ERK pathway, the essential linkers between epidermal growth factor receptors and other receptor tyrosine kinases, and the MAPK cascade include adaptor protein Grb2, a Son of Sevenless (SOS) family of guanine nucleotide exchange factors, and a small GTP binding protein Ras (Figure 1A). The MAPK cascade begins with MAPKKK (represented by c-Raf) which phosphorylates and activates MEK1 and MEK2 (MAPKKs). MEKs eventually phosphorylate, and thereby activate p44 MAPK and p42 MAPK, also known as ERK1 and ERK2, respectively (Lavoie et al., 2020; Stokoe et al., 1994). The activated ERKs then translocate to the nucleus where they phosphorylate and transactivate various transcription factors such as Elk-1, c-Jun and c-Fos, thereby altering gene expression to promote growth, differentiation, or mitosis. The ERK/MAPK pathway also directly regulates translational machinery, for example by stimulating the activity of both ribosomal S6 protein kinases (RSKs; RSK1-4 in humans) (Carriere et al., 2008) and MAPK-interacting kinases (MNKs; MNK1 and 2 in humans) (Buxade et al., 2008; Fukunaga and Hunter, 1997; Waskiewicz et al., 1997). MNKs interact with eIF4G and phosphorylate eIF4E at Ser209, a site that increases the oncogenic potential of eIF4E (Topisirovic et al., 2004) and facilitates translation of specific mRNAs related to migration, metastasis and inflammation (Furic et al., 2010; Pyronnet et al., 1999; Robichaud et al., 2015). Following the stimulation of the ERK pathway, activated RSKs phosphorylate rpS6, eIF4B, eEF2K, and PDCD4, which are all important translational regulators (reviewed in (Bhat et al., 2015; Robichaud and Sonenberg, 2017)). RSKs have also been implicated in the regulation of other signaling pathways involved in growth control, stress-response and cancer including the regulation of mTORC1 (reviewed in (Roux and Topisirovic, 2018)). For example RSKs have been shown phosphorylate and inhibit tuberous sclerosis complex 2 (TSC2) that acts as the negative regulator of mTORC1 signaling (Roux et al., 2004) (Figure 1A).

It has been shown that alterations in genomic sequences, protein levels, stoichiometry, and/or activity of eIFs and other components of the translational apparatus and relevant signaling cascades, as well as in cis-regulatory elements of mRNAs, can circumvent the stress-induced translational shutdown that these pathways impose by allowing selective recruitment of mRNAs, rewiring translational control of mRNA cis-regulatory elements, and/or enabling alternative start codon selection (Kovalski et al., 2022; Robichaud et al., 2019; Sriram et al., 2018). Naturally, this leads to various pathologies. Overexpression of eIF4F complex components, for example, has been observed in various cancer entities (Bhat et al., 2015; De Benedetti and Harris, 1999;

Lazaris-Karatzas et al., 1990; Ruggero, 2013; Shuda et al., 2000; Truitt and Ruggero, 2016). In addition to eIF4F components, dysregulation of the multi-subunit eIF3 complex is also involved in oncogenesis. Ten of the twelve eIF3 subunits have been linked to human cancers, many due to overexpression (a, b, c, d, g, h, m or i), some due to underexpression (e and f) (reviewed in (de la Parra et al., 2018b; Gomes-Duarte et al., 2018; Hershey, 2015; Valasek et al., 2017; Zhang et al., 2007)). In this regard it is worth stressing that some eIF3 subunits have been shown to directly interact with specific mRNAs (Lee et al., 2015), eIF3d together with DAP5 was shown to facilitate alternate form of cap-dependent mRNA translation (de la Parra et al., 2018a), and eIF3k was recently proposed to serve as a regulator of the balanced ribosome content (Duan et al., 2023). Despite all these relevant observations, the exact mechanism(s) by which eIF3 affects various pathologies is virtually unknown. Moreover, previous studies that investigate the effect of eIF3 in specific diseases focus on altered levels of only one of the eIF3 subunits, while neglecting the need to consider the context of altered expression of the entire eIF3 complex.

Here, we draw attention to this unfortunate trend. eIF3 is the largest and most complex eIF of all eIFs, it is modular in nature (Figure 1B) (reviewed in (Cate, 2017; Valasek et al., 2017; Wolf et al., 2020)), and plays multiple roles not only in translation initiation, but also in termination, ribosomal recycling and stop codon readthrough (Beznosková et al., 2013; Beznosková et al., 2015; Pisarev et al., 2007; Poncova et al., 2019). Each of these roles may be regulated differently by individual subunits and/or their combinations, making it practically impossible to study them in isolation. Eight eIF3 subunits (a, c, e, f, h, k, l and m) form a structural scaffold called the PCI (**P**roteasome, **C**OP9, e**I**F3) / MPN (**M**pr1-**P**ad1 **N**-terminal) octamer, whereas the remaining four non-octameric subunits (b, d, g and i) are likely to be more flexible. The essential subunits b, g, and i form a separate module that is connected to the octamer *via* the C-terminal domain (CTD) of eIF3a; together they are called YLC for **Y**east **L**ike **C**ore (Wagner et al., 2016). The eIF3d subunit is located on the eIF3 periphery and is attached to the octamer primarily via eIF3e, but partly also *via* eIF3a and c (Bochler et al., 2020; Brito Querido et al., 2020). On the 40S subunit, the octamer is positioned close to the mRNA exit site, whereas the mobile YLC shuffles between the mRNA entry site and the subunit interface during the AUG selection process (des Georges et al., 2015; Llacer et al., 2021; Llácer et al., 2018; Simonetti et al., 2020).

We recently reported a comprehensive *in vivo* analysis of the modular dynamics of the human eIF3 complex (Wagner et al., 2020; Wagner et al., 2014; Wagner et al., 2016). Using a systematic individual downregulation strategy, we showed that the expression of all 12 eIF3 subunits is interconnected such that perturbance of the expression of one subunit results in the down-regulation of entire modules leading to the formation of partial eIF3 subcomplexes with limited functionality (Herrmannova et al., 2020). Here we took advantage of this knowledge to examine the specific effect of

selected eIF3 subcomplexes on the translation efficiency, transcriptome-wide, in HeLa cells.

METHODS

Cell lines, culture conditions and transfection

HeLa cells (ATCC: CCL2) were grown at 37 °C and 5% CO2 in Ø 15 cm dishes in DMEM (Sigma, cat #D6429) supplemented with 10% FBS (Gibco, cat # 10270-106). Twenty-four hours after seeding, cells were transfected with the ON-TARGETplus siRNA cocktail system from Dharmacon at a final concentration of 5 nM. Catalog numbers for all siRNAs used in this study are listed in Supplementary Table S1. INTERFERin (Polyplus, cat # 101000016) was used as a transfection reagent, 100 µl per dish. Cells were harvested 72 hours after transfection at approximately 80% confluency and cytoplasmatic lysates were prepared as described previously (Herrmannova et al., 2020). For monitoring levels of phosphorylated c-Jun protein, cytoplasmatic and nuclear lysates were prepared using NE-PER™ Nuclear and Cytoplasmic Extraction Reagents from Thermo Scientific™.

Ribosome profiling (Ribo-Seq) and RNA-seq library preparation

For **footprint (FP) libraries** cycloheximide was added to a final concentration of 100 µg/ml 1 min prior to harvesting. Cells were washed with ice cold 1x PBS and lysed in buffer A (10 mM HEPES [pH 7.5], 62.5 mM KCl, 2.5 mM $MgCl_2$, 1 mM DTT, 1 mM PMSF, 1 µg/ml Aprotinin, 1 µg/ml Leupeptin, 1 µg/ml Pepstatin, Complete Mini EDTA-free [Roche, cat # 11836170001] – 1 tablet/5 ml, 1% Triton X-100, 100 µg/ml Cycloheximide) on the dish. The resulting lysate was collected and cleared by centrifugation. Aliquots of twelve absorbance units (AU) OD_{260} of WCE were flash frozen in liquid nitrogen and used for control polysome profile and footprint isolation. An aliquot of 1 mg total protein was taken for control western blot, and another 200 µl aliquot was mixed with 1 ml of RNA Blue (TopBio, cat # R013) and taken for RNA isolation and control qPCR. When the lysate passed all three control experiments (polysome profile, western blot, qPCR), one aliquot of 12 AU OD_{260} was thawed on ice, digested with 5 µl RNAseI (Ambion, cat # AM2295) for 30 min at 24 °C with mild shaking (300 rpm) and inactivated with SuperaseIN (Ambion, cat #AM2696). 80S ribosomes were separated by high-velocity sedimentation through a 5% to 45% sucrose gradient at 39,000 rpm for 2.5 h using the SW41Ti rotor. The gradients were scanned at 254 nm to visualize the ribosomal species and fractions containing 80S ribosomes were collected and mixed with RNA Blue. RNA was isolated according to vendor's instructions, FP RNA was size selected on 15% TBE-Urea PAGE (Biorad, cat # 3540092) in range 20-40 nt and footprint library was prepared according to (Ingolia et al., 2012). FP libraries were sequenced on NovaSeq6000 (Illumina) with read length 50 nt.

For **mRNA libraries** the growth media was aspirated and cells were harvested into 5 ml of RNA Blue per Ø 15 cm dish. RNA was isolated according to vendor's instructions. mRNA was isolated from the total RNA using Poly(A)purist MAG kit (Ambion, cat #

AM1922), fragmented using RNA Fragmentation Reagents (Ambion, cat # AM8740) and size selected on 15% TBE-Urea PAGE in range 50-100 nt. Size selected mRNA was then dephosphorylated and library was prepared using SMARTer smRNA-Seq Kit (TAKARA, cat # 635029) according to vendor's instructions. mRNA libraries were sequenced on NovaSeq6000 (Illumina) with read length 150 nt.

RNA isolation, reverse transcription and qPCR

Total RNA was isolated using RNA Blue reagent (TopBio, cat # R013) 72 h post-transfection according to the manufacturer's instructions. After DNase I digestion (NEB, cat # M0303L), cDNA was synthesized from 1µg RNA using the High-Capacity cDNA Reverse Transcription Kit (Applied Biosystems, # 4368813). qPCR was performed in triplicates using 5× HOT FIREPol EvaGreen qPCR Mix Plus (Solis BioDyne # 08-25-00020). The obtained data were normalized to ALAS1 mRNA levels and non-transfected control. All qPCR primers are listed in Supplementary Table S2.

Western blotting

All samples were resolved using SDS-PAGE followed by western blotting. All primary antibodies used in this study are listed in Supplementary Table S3. The signal was developed using SuperSignal West Femto Maximum Sensitivity Substrate (Thermo Scientific, cat # 34096) and detected in a G-Box imager (Syngene) using a series of varying exposure times.

Polysome profiles

One aliquot of 12 AU OD_{260} was thawed on ice and separated by high-velocity sedimentation through a 5% to 45% sucrose gradient at 39,000 rpm for 2.5 h using the SW41Ti rotor. The gradients were scanned at 254 nm to visualize the ribosomal species.

Analysis of Sequencing Data

We processed the ribosome **footprint libraries** as follows. Adapter sequence "CTGTAGGCACCATCAAT" and all sequences 3' of the adapter were trimmed from the 3' end of each read by Cutadapt v. 3.5 (Martin, 2011). Flanking Ns were trimmed from both 5' and 3' ends of each read. Reads without adapter sequence and reads shorter than 15 nt after trimming were discarded. Next, rRNA and tRNA reads were discarded after alignment with Bowtie2 v. 2.4.4 (Langmead and Salzberg, 2012). For rRNA, we used RNA5S1, RNA5-8SN5, RNA18SN5 and RNA28SN5 from NCBI (Sayers et al., 2022), and ENSG00000211459 and ENSG00000210082 from Ensembl (Howe et al., 2021). For tRNA we used all human tRNA sequences from tRNAdb (Juhling et al., 2009) and all high confidence hg38 tRNA sequences from GtRNAdb (Chan and Lowe, 2016). Remaining reads were aligned to genome and transcriptome from Ensembl (GRCh38.p13, annotation release 104) by the STAR aligner v. 2.7.9a_2021-06-25 (Dobin et al., 2013)

using local alignment with 10% mismatches, and with indels and soft clipping allowed for transcriptomic alignment. Gene counts were counted from genomic alignment using Samtools index v. 1.13 (Danecek et al., 2021) and Htseq-count v. 0.13.5 (Anders et al., 2015) within CDS regions. Transcriptomic alignments were further processed using MANE Select set from MANE project v. 0.95 (Morales et al., 2022) and custom programs "mane2ensembl_gtf", "filter_reverse_reads", "filter_ambiguous_genes" and "select_transcripts". See Supplementary Spreadsheet S1 for detailed overview of raw read processing.

The **RNA-seq libraries** were processed the same as above, except that raw read processing by Cutadapt had to be adapted to different library construction method (SMARTer smRNA-Seq Kit, TAKARA). In particular, first 3 nucleotides on the 5' end were removed, and poly(A) sequence (10xA) was trimmed from the 3'end.

Quality checks were done by FastQC v. 0.11.9 (Andrews, 2010) and Ribo-seQC v. 1.1 (Calviello et al., 2019). Triplet periodicity was checked on transcriptomic alignments using custom modified riboWaltz (Lauria et al., 2018) and a custom script "Triplet_periodicity.R". Gene counts were used to check correlation between replicates using a custom script "Correlation-samples.R". Read length counts were used to check read length distribution using a custom script "Lengths.R".

PCA plot, sample distances clustering and the differential expression analysis were performed on gene counts by DESeq2 (Love et al., 2014) with biomaRt library (Durinck et al., 2009) used to download gene annotations. Differential translation efficiency (TE) values between NT and the knock-downs were calculated as described in (Chothani et al., 2019). The p_{adj} threshold for differentially translated transcripts was set to 0.05. For details see custom script "Differential analysis.R". Results of differential expression analysis were further used to generate heatmap and scatterplots of differentially expressed genes and genes with defined p-adjusted value were used to analyze dependency between mRNA characteristics and changes in TE using custom scripts "Significant_TE_heatmap.R", "Significant_TE_intersection.R" and "Correlation-features.R". To get mRNA characteristics we used MANE Select set to select a single representative transcript for each protein-coding gene. uORF database uORFdb (Manske et al., 2023) was used to get number of ATG uORFs per mRNA.

Metagene analysis was done as described in (Lin et al., 2020), but 5' ends of reads were used instead of P-sites. Samtools and custom programs "transcripts_startstop_positions", "read_counts" and "region_readcounts" were used to get read counts relative to the start codon. These were normalized to a number of reads in a region starting 75 bases after the start codon and ending 15 bases before the stop codon and averaged over the samples. Only transcripts that met the following parameters were considered: CDS longer than 450 nt and RPKM higher than 10. Weighted counts of biological replicates were further used to compute average read counts for each sample. Moving average method was used with a 21 bases window size.

For footprint coverage plots of individual mRNAs, MANE transcripts of examined genes (ENST00000674920-ATF4; ENST00000258149-MDM2; ENST00000251849-RAF1) were selected. Reads were counted for each position using Samtools and a custom script read_counts and normalized to number of read counts over all positions of transcript. Weighted counts of biological replicates were further used to compute average read counts for each sample. Graphs were smoothened with a sliding window of 30nt. All used custom scripts are available on Github.

KEGG/GO pathway enrichment analysis

We analyzed enrichment of the differentially translated transcripts in KEGG pathways (Kanehisa and Sato, 2020) and Gene Ontology (Ashburner et al., 2000; Gene Ontology, 2021) using Enrichr (Kuleshov et al., 2016), ShinyGO v0.741 (Ge et al., 2020) and KEGG Mapper Search (Kanehisa et al., 2022). Venn diagrams were created using InteractiVenn (Heberle et al., 2015).

Analysis of Gene Signatures

To assess changes in the regulation of known gene signatures in the eIF3 KDs, empirical cumulative distribution functions (ECDFs) of $\log_2$ fold changes in FP and total mRNA were plotted independently. Fold change ECDFs for genes belonging to a particular signature were compared to those for all other genes, and differences in distributions were calculated at the quantiles. Significant directional shifts between the signatures and the background were identified using the Wilcoxon rank-sum test.

RESULTS

High quality sequencing libraries prepared from HeLa cells expressing different eIF3 subcomplexes.

To investigate the impact of different human eIF3 subunits and partial eIF3 sub-complexes, which arise in cells as a result of unbalanced eIF3 expression, on translational efficiency transcriptome-wide, we performed Ribo-Seq together with RNA-Seq, which allowed us to draw conclusions about gene expression at the transcriptional and translational levels and their interdependence. In particular, using the siRNA technology, we examined HeLa cells with reduced levels of eIF3d, eIF3e or eIF3h subunits and cells treated with non-targeting (NT) siRNA. These eIF3 subunits were selected because the eIF3d depletion leads to a reduction in protein levels of only eIF3d and leaves the rest of the eIF3 complex intact, whereas downregulation of eIF3e or eIF3h generates partial eIF3 subcomplexes as previously described (Wagner et al., 2016). Specifically, targeting eIF3e with siRNA results in reduced protein levels of eIF3e, eIF3d, eIF3k and eIF3l, whereas downregulation of eIF3h produces a partial eIF3 complex lacking subunits eIF3h, eIF3k and eIF3l (Figure 1B). In terms of impact on cell growth, both eIF3d^{KD} and eIF3e^{KD}

strongly reduce proliferation, while the effect of eIF3h^{KD} is only moderate (Supplementary Figure 1A) (Wagner et al., 2016).

We first performed several control experiments with aliquots of cell lysates made to prepare individual Ribo-Seq libraries to document an efficient downregulation of the targeted eIF3 subunit, as well as the expected phenotype (Wagner et al., 2016). Using qPCR, we measured mRNA levels of the siRNA targeted eIF3 subunits (eIF3d, eIF3e, eIF3h), as well as eIF3b as a negative control and a housekeeping gene ALAS1 for normalization purposes. Routinely, a difference of 4 to 5 cycles was achieved for each downregulated subunit, corresponding to ~16–32 fold decrease in mRNA levels; the mRNA levels of the control subunit eIF3b remained unchanged (Figure 2A); note that Figure 2A summarizes qPCR results for all samples used to generate of Ribo-Seq and RNA-Seq libraries.

Next, we determined protein levels of selected eIF3 subunits by Western blotting. Protein levels of all eIF3 subunits targeted individually by siRNA were strongly reduced (Figure 2B). Depletion of eIF3e also induced a marked decrease in the eIF3d protein level (Figure 2B) and eIF3k and eIF3l (data not shown) as previously reported (Wagner et al., 2016). Finally, we performed polysome profiling to assess the impact on translation and obtained essentially the same results as before (Wagner et al., 2016). The eIF3d^{KD} showed the most pronounced defect in translation initiation, marked by a robust increase of the 80S monosome peak and a concomitant decrease of polysome content, similar to eIF3e^{KD}, while eIF3h^{KD} had only a modest effect on polysome formation (Supplementary Figure 1B).

Ribo-Seq libraries were generated from each knock-down and NT control in three biological replicates as described in (Ingolia et al., 2012). RNA-Seq libraries were prepared in four biological replicates using the SMARTer smRNA-Seq Kit to normalize for mRNA levels and calculate translational efficiency (TE). Both Ribo-Seq and RNA-seq libraries were highly reproducible as shown by the Spearman correlation coefficient (Supplementary Figure 2A). All Ribo-Seq libraries showed a similar read length distribution with a prominent peak at 30 – 32 nt and an expected 3 nt periodicity in coding sequences (CDS) (Supplementary Figure 2B-C and Figure 2C). As expected, Ribo-seq libraries were strongly enriched for CDS reads compared to RNA-Seq libraries (Supplementary Figure 2D – E). The PCA plot and hierarchical clustering (Figure 3A and Supplementary Figure 3A) showed clustering of the samples into two main groups: Ribo-Seq and RNA-seq, and also into two subgroups; NT and eIF3h^{KD} samples clustered on one side and eIF3e^{KD} and eIF3d^{KD} samples on the other. These results suggest that eIF3h depletion impacts the translatome differentially than depletion of eIF3e or eIF3d.

eIF3 subcomplexes alter translation efficiency of a large proportion of genes

Using the R DESeq2 package (Love et al., 2014), we identified transcripts with significantly altered TE ($P_{adjusted} < 0.05$) for each knock-down compared to the NT control

(Figure 3B – D, Supplementary Spreadsheet S2), henceforth referred to as Differential Translation Efficiency Genes (DTEGs) (Chothani et al., 2019). In total, we identified 21 DTEGs in eIF3h^{KD} (19 downregulated and 2 upregulated), 1180 DTEGs in eIF3e^{KD} (622 down and 558 up), and 1971 DTEGs in eIF3d^{KD} (1040 down and 931 up) out of a total of 17520 genes that were assigned TE values.

The number of DTEGs in each knock-down correlated well with the severity of the overall phenotype and with the impact on global translation, as judged from the polysome profiles. eIF3d^{KD} with the strongest decrease in polysomes had the highest number of DTEGs, whereas eIF3h^{KD} with only 21 DTEGs had a marginal effect on polysome formation (Supplementary Figure 1B). Consistently, the overall distribution of fold-changes in TE showed most pronounced changes in eIF3d^{KD} (Supplementary Figure 3B). It should be noted, however, that in contrast to polysome profiling, differential expression analysis of Ribo-Seq data normalizes out global changes in translational rates, and reveals only specific shifts of ribosome localization on individual mRNAs between the NT and KD datasets. In agreement, all three knock-downs showed an increase in TE for approximately half of the affected genes, reflecting specific regulation rather than simply non-specific global translation shutdown.

Interestingly, there is a considerable overlap between the knock-downs studied, such that only 1045 DTEGs are unique for eIF3d^{KD} and the rest (926) are shared with other two knock-downs; in particular 923 with eIF3e^{KD} and 21 with eIF3h^{KD} – in the latter case, the overlap reaches 100% (Figure 3E, Supplementary Figure 4A – C). Remarkably, eIF3d^{KD} affects neither the expression of any other eIF3 subunit nor the integrity of the eIF3 complex, yet it has the most pronounced impact on translation (Wagner et al., 2016), correlating well with the highest number of DTEGs identified. In case of eIF3e^{KD}, only 257 DTEGs are unique and the rest (923) are shared with eIF3d^{KD}, 18 of which are also shared with eIF3h^{KD} (Figure 3E, Supplementary Figure 4A – C). The eIF3 subcomplex formed in eIF3e^{KD} lacks subunits e, k and l and partially also eIF3d (Wagner et al., 2016) – the significantly reduced protein levels of eIF3d are evident in Figure 2B. Thus, it is not surprising that the DTEGs identified in eIF3e^{KD} largely overlap with those identified in eIF3d^{KD}; in fact, this result supports the robustness and accuracy of this approach. The fact that the magnitude of the knock-down effect is bigger in eIF3d^{KD} over eIF3e^{KD} is discussed below.

eIF3d^{KD} and eIF3e^{KD} increase TE of mRNAs encoding proteins associated with membrane organelles

To analyze enrichment in KEGG pathways and GO Biological Processes in a meaningful way, we analyzed the DTEGs divided not only into upregulated and downregulated groups, but also into specific subgroups – eIF3d^{KD} “all”, eIF3e^{KD} “all”, eIF3d^{KD} “unique”, eIF3e^{KD} “unique” and eIF3d^{KD}/eIF3e^{KD} “common” (Figure 3E – G). To disentangle the effects of transcriptional and translational regulation, we also investigated translationally

exclusive DTEGs whose mRNA abundance did not change significantly and therefore the change in TE can be attributed solely to translational regulation; eIF3d^{KD} "translation only" and eIF3e^{KD} "translation only", as well as translationally buffered DTEGs whose mRNA abundance changes in opposite direction than translational regulation, i.e. mRNA increases but TE decreases so the net protein production is not changed or even decreased; eIF3d^{KD} "buffered" and eIF3e^{KD} "buffered"(Supplementary Figure 4D – F). For schematic illustrating classification of genes based on fold changes of footprints (FP), mRNA, and TE, see Supplementary Figure 4G – H (adopted from (Chothani et al., 2019) with permission).

Analysis of DTEGs upregulated in eIF3d^{KD} and eIF3e^{KD} showed similar results for almost all groups analyzed (eIF3d^{KD} "all", "unique", and "translation only", eIF3d^{KD}/eIF3e^{KD} "common", as well as eIF3e^{KD} "all" and "translation only") (Figure 4A, B, and Supplementary Figure 5A), with the strongest enrichment in the KEGG "Lysosome" and "Protein processing in endoplasmic reticulum" pathways. The majority of DTEGs in these pathways were solely translationally regulated meaning that their mRNA levels stayed unchanged while the TE increased. For example, for the KEGG pathway "Lysosome", more than 70% (i.e. 37 out of the 51) DTEGs upregulated in the eIF3d^{KD} "all", fall into the eIF3d^{KD} "translation only" group. This suggests that when translation initiation is compromised by eIF3d/e^{KD}, cells may increase protein degradation and turnover by translationally upregulating lysosomal and ER proteins. Interestingly and in accord with our results, Lin et al. detected increased lysosomal load in MCF-10A cells downregulated for eIF3e (Lin et al., 2020). They speculated that this is due to the need to clear defective mitochondria. In support, we also found enrichment of mitochondria-associated DTEGs, especially mitochondrial ribosomal proteins (see below).

As for the eIF3d^{KD} "unique upregulated" DTEGs, we identified one interesting and unique KEGG pathway, the ABC transporters (Supplementary Figure 5A, in green). A total of 12 different ABC transporters had elevated TE (9 of them are unique to eIF3d^{KD}, while 3 were also found in eIF3e^{KD}), 6 of which (ABCC1-5, ABCC10) belong to the C subfamily, known to confer multidrug resistance with alternative designation as multidrug resistance protein (MRP1-5, MRP7) (Sodani et al., 2012). Interestingly, all six of these ABCC transporters were upregulated solely at the translational level (Supplementary Spreadsheet S2).

eIF3e^{KD} increases production of ribosomal proteins

Interestingly, the KEGG pathway "Ribosome" and GO terms connected with translation and ribosome biogenesis were enriched amongst DTEGs upregulated specifically in eIF3e^{KD} "unique upregulated" DTEGs (Figure 4C and Supplementary Figure 5B). We then compared the significance of enrichment for "Ribosome" KEGG term between eIF3e^{KD} and eIF3d^{KD} "all upregulated" groups. This was the only case where a term or a pathway was more significantly enriched in eIF3e^{KD} (P = 5.199E-10) than in eIF3d^{KD} (NS, P =

0.1183) (Supplementary Figure 5A, in green). Intrigued by this result, we filtered out all ribosomal proteins (RPs) from our data set (according to HGNC database, (Tweedie et al., 2021)), regardless of the TE changes, which consisted of 89 cytoplasmic and 77 mitochondrial RPs, and analyzed them separately (Supplementary Spreadsheet S2). In total, we identified 32 RPs with significantly changed TE in eIF3e^{KD} (14 cytoplasmic and 18 mitochondrial) and only 16 in eIF3d^{KD} (9 cytoplasmic and 7 mitochondrial). Moreover, all the cytoplasmic RPs with increased TE in eIF3e^{KD} (and most mitochondrial ones) were upregulated solely at the translational level and their mRNA levels were not changed. We selected several RPs with different combinations of changes in TE or FP or mRNA levels in both eIF3e^{KD} and eIF3d^{KD} (Figure 4D) and subjected them to western blotting. All ribosomal proteins tested showed visibly increased protein levels in both eIF3e^{KD} and eIF3d^{KD} (Figure 4E), while their mRNA levels remained unchanged (Supplementary Figure 5C). For some RPs (RPS2, RPS3), the increase was more pronounced in eIF3e^{KD}. Overall, our results suggest that eIF3e and, to some extent, its binding partner eIF3d maintain control over production of RPs in the cell. A similar role has recently been attributed to eIF3k, which has been shown to specifically repress the synthesis of the small ribosomal protein RPS15A, and cells depleted of eIF3k showed increased ribosomal content (Duan et al., 2023). As mentioned above, targeting eIF3e with siRNA results in co-downregulation of not only eIF3e and eIF3d, but also of eIF3k and eIF3l (Wagner et al., 2016).

In addition to mitochondrial RPs, we also observed increased TE for several other mitochondrial proteins from the Complex I, Complex IV and Complex V (KEGG term Oxidative phosphorylation hsa00190; rank 17; #of genes 12 out of 134; p = 0.0003431) in eIF3e^{KD}, but many of these transcripts, mainly from the Complex I, are encoded by mitochondrial DNA and translated in mitochondria directly, so these results should be verified by Mitoribosome profiling, as the traditional Ribo-Seq method is not suitable for this (Pearce et al., 2021).

Because RPs and other components of the translational machinery frequently harbor 5' terminal oligopyrimidine (TOP) motifs that render their translation highly sensitive to mTORC1 (Philippe et al., 2020; Stolovich et al., 2002), we first investigated whether mTORC1 translation is affected in eIF3d^{KD} or eIF3e^{KD} but found no significant change in TE for any mTORC1 components. Next, we examined the effect of depletion of eIF3 subunits on translation of all known TOP mRNAs. We observed that transcripts harboring TOP motifs (Philippe et al., 2020) were significantly translationally activated in eIF3d^{KD} and eIF3e^{KD}, but not in eIF3h^{KD} (Figure 5A - C). Interestingly, the effect of eIF3d^{KD} and eIF3e^{KD} on translation of non-TOP mRNAs that are mTORC1-sensitive (Gandin et al., 2016) differed from what was observed for TOP mRNAs, as non-TOP transcripts were predominantly translationally offset (buffered), such that translation efficiency was increased to maintain a constant level of polysome association despite decreased total mRNA abundance (Supplementary Figure 6A - C). Together, these findings suggest that

eIF3e and eIF3d may play a role in tempering translation of TOP mRNAs under normal cellular conditions, and that the loss of these eIF3 subunits has distinct impact on the translatome as compared to mTORC1.

eIF3d^{KD} and eIF3e^{KD} decrease translation efficiency of the key components of the MAPK/ERK and other signaling pathways implicated in cancer

The eIF3d^{KD} or eIF3e^{KD} "all downregulated" and eIF3d^{KD}/eIF3e^{KD} "common downregulated" groups were enriched for a similar set of KEGG pathways (Figure 6A and Supplementary Figure 7A). The effect is generally stronger for eIF3d^{KD}, which simply means that this knock-down has a higher number of DTEGs in the same pathway than eIF3e^{KD} (for example MAPK signaling pathway: 42 vs. 30 DTEGs for eIF3d^{KD} vs. eIF3e^{KD}, respectively). Therefore, we focused primarily on DTEGs identified in eIF3d^{KD} "all" (Figure 6A and Supplementary Figure 7A). Most of the top ten KEGG results are related to and/or encompass the MAPK signaling pathway (Supplementary Figure 7B), like Chronic myeloid leukemia and the Neurotrophin signaling pathway. Depletion of eIF3d affected multiple components of the MAPK signaling pathway, which plays a critical role in the regulation of cell proliferation (Zhang and Liu, 2002) and cancer development and progression (reviewed in (Dhillon et al., 2007)). These include the docking protein Grb2 (encoded by *GRB2*) and guanine nucleotide exchange factor Sos (*SOS1*), through kinases c-Raf (*RAF1*), MEK1 (*MAP2K1*), Erk2 (*MAPK1*), MNK1 (*MKNK1*), Rsk2 (*RPS6KA3*), to the transcription factor CREB (*ATF4*). In addition, Rac1 and PAK1, that activate c-Raf by increasing phosphorylation of Ser338 (King et al., 1998) were also significantly affected (Figure 1A, Supplementary Figure 7C and Supplementary Spreadsheet S2). Consistent with the observed translational suppression of MNK1, which phosphorylates eIF4E (Waskiewicz et al., 1997), mRNAs that critically depend on phospho-eIF4E levels (Karampelias et al., 2022) were translationally offset in eIF3d^{KD} and eIF3e^{KD} cells, such that translation efficiency was decreased to maintain a constant level of polysome association despite increased total mRNA abundance (Supplementary Figure 8A - B).

Consistently, Gene Ontology (GO) analysis revealed strong association of downregulated DTEGs with biological processes "protein phosphorylation" and "regulation of transcription" and the molecular function term "protein serine/threonine kinase activity" (Supplementary Figure 9A – B). Key integrin-mediated signaling proteins that were implicated in cancer cell plasticity, adhesion, migration and survival (reviewed in (Cooper and Giancotti, 2019)) also had significantly decreased TE, specifically, proto-oncogenes Crk (*CRK*) and Crk-L (*CRKL*), *PRKCA* – a catalytic subunit of PI3-kinase, Rac1 GTPase (*RAC1*), JNK2 (*MAPK9*), as well as Abl1 kinase (*ABL1*) and BCR activator of Rho-GEF (*BCR*). The TGF-beta signaling, important for a wide range of cellular processes as well as for tumor cell invasion, metastasis, and resistance to chemotherapy (reviewed in (Colak and Ten Dijke, 2017)), was affected at the level of the intracellular

transducer Smad4 (*SMAD4*) and receptor activated SMADs, namely Smad3 (*SMAD3*) and Smad5 (*SMAD5*) and TGF beta (*TGFB3*) itself. The NFkB pathway, a regulator of immune and inflammatory responses (Liu et al., 2017), also implicated in cancer cell proliferation, survival, angiogenesis and plasticity (reviewed in (Xia et al., 2014)), was downregulated at the level of NFkB (*NFKB1*) itself and IKK kinase (*CHUK*). Notably, a direct link between activation of NFkB and eIF3 has very recently been described (She et al., 2023). Finally, the canonical Wnt signaling pathway, which shapes the stem cells-like properties of cancer cells and boosts proliferation (reviewed in (Zhang and Wang, 2020)), was downregulated at the level of a protein Dishevelled (*DVL3*) and GSK3 beta kinase (*GSK3B*). Physiological relevance of all these hits remains to be seen; for the complete list of all DTEGs, please see Supplementary Spreadsheet S2.

eIF3d^{KD} and eIF3e^{KD} reduce protein levels of key components of the activated MAPK/ERK pathway.

Interestingly, more than half (26 of the 42) downregulated DTEGs belonging to the MAPK signaling pathway can be classified as translationally buffered; i.e., their mRNA levels increase while their TE decreases (Kusnadi et al., 2022). However, this is not a typical case of translational buffering because transcriptional upregulation is not only nullified by translational repression, but completely overruled, so that the total number of FPs is also reduced. To verify that the reduction in TE and FP counts is indeed manifested by a reduction in cellular protein levels, we selected a set of genes with different combinations of changes in TE or FP or mRNA levels, including translationally exclusive and translationally buffered genes, as well as genes with unchanged TE, and subjected them to western blotting (Figure 6B - C).

We found, that AKT1, GRB2, MAP2K1 (MEK1), RPS6KA1 (RSK1), RPS6KA3 (RSK2), RAF1 and SOS1 had visibly decreased protein levels in eIF3d^{KD} and some of them also in eIF3e^{KD}. The only exception, which showed no changes in protein levels, was PAK1, with decreased TE, FP counts, as well as mRNA levels. However, this discrepancy could be explained by the non-specificity of the available polyclonal antibody that cross-react with PAK1-related proteins PAK2 and PAK3. Another interesting exception is the transcription factor c-Jun, which showed increased mRNA and FP levels, unchanged TE, but robust increases in protein levels in all three knock-downs (Figure 6C). The mRNA levels of all selected genes were verified by qPCR, showing a good correlation with our sequencing data; whereas PAK1 showed significant decrease, JUN mRNA was significantly increased in both eIF3d^{KD} and eIF3e^{KD} (Supplementary Figure 9C). To assess the functional consequences of the downregulation of MAPK pathway components, we examined the phosphorylation status of effector kinases ERK1/2, which directly phosphorylate several transcription factors including c-Jun (Leppa et al., 1998). As with other MAPK proteins, ERK1/2 expression was reduced in eIF3d^{KD} and eIF3e^{KD}, but its phosphorylation at activation sites Thr202/Tyr204 was unexpectedly increased in

all three knock-downs (Figure 6D). Next, we examined the phosphorylation status of the upregulated c-Jun protein. As phosphorylated c-Jun translocates to nucleus to activate transcription of specific genes, we performed western blot of both cytoplasmatic and nuclear fractions. In accord with increased ERK1/2 phosphorylation, c-Jun was found to be activated by phosphorylation at Ser63 and largely accumulated in the nucleus (Figure 6E). Thus, despite reduced MAPK pathway protein levels, MAPK signaling appears to be activated when eIF3 function in translation is compromised.

Intact eIF3 contributes to translational regulation of ATF4 and MDM2

Knocking down eIF3h generates an eIF3 subcomplex lacking eIF3h and two nonessential subunits eIF3k and eIF3l (Figure 1B), having only negligible impact on overall translation. Accordingly, we identified 19 transcripts whose TE was decreased and only 2 transcripts whose TE was increased compared to the NT control (Figure 3D). Given the low number of DTEGs, we observed no significant enrichment of any KEGG pathway within the upregulated DTEGs and only a few significant enrichments for the eIF3h^{KD} "all downregulated" DTEGs in pathways like "Prostate cancer", "Viral carcinogenesis" or "PI3-Akt signaling pathway", all of which included only two common hits – MDM2 and ATF4 (Figure 7A, Supplementary Table S4). Additionally, we also noticed enrichment of GO terms associated with ubiquitination (Figure 7B, Supplementary Table S5), which was mainly due to the MDM2, WAC, RNF10, RMND5A, USP38 and ZRANB1 genes, all of which showed decreased TE. MDM2, WAC, RNF10 and RMND5A are all E3 ubiquitin ligases while USP38 and ZRANB1 are de-ubiquitinases. Note that all of the above downregulated DTEGs are common for all three knock-downs.

Perhaps the most interesting of these genes is the proto-oncogene MDM2, an E3 ubiquitin ligase that acts as a negative regulator of the p53 protein (Marine and Lozano, 2010), whose overexpression has been reported in many different cancer types (Rayburn et al., 2005). We did confirm that the MDM2 protein levels were reduced in all three knock-downs (Figure 7C).

An equally interesting DTEG is ATF4, which is among the top 10 most significant DTEGs in all three knock-downs (Figure 3B - D). In eIF3h^{KD}, it can be classified as a translationally buffered gene because it has strongly upregulated mRNA levels, but this increase is not accompanied by a concomitant increase in the FP count, thereby resulting in decreased TE. In eIF3d^{KD} and eIF3e^{KD}, it is even significantly translationally repressed (FPs are decreased). Using qPCR, we confirmed its transcriptional upregulation in all three knock-downs (Supplementary Figure 10A). Because ATF4 protein levels are on the verge of the western blot detection limit under non-stress conditions, we examined whether all three knock-downs tested had any effect on ATF4 induction upon 3 hour-long ER stress provoked by 1mM Thapsigargin (Harding et al., 2000). Indeed, stress-mediated ATF4 induction was almost abolished in eIF3d^{KD} and eIF3e^{KD}, and strongly decreased in eIF3h^{KD} (Figure 7D). This differential effect correlates well with our sequencing data,

where the decrease in TE was also stronger in eIF3d^{KD} and eIF3e^{KD}. ATF4 protein levels in DMSO control are shown as a no stress reference. Overall, these findings further confirm that an intact eIF3 complex is required for proper translational control of ATF4, as we and others have previously suggested (Guan et al., 2017; Hronova et al., 2017; Mukhopadhyay et al., 2023; Shu et al., 2022; Wagner et al., 2020), and as discussed below.

As both *ATF4* and *MDM2* are known to contain uORFs in their 5' UTR that regulate their translation under stress vs. non-stress conditions (Akulich et al., 2019; Dey et al., 2010; Lu et al., 2004; Vattem and Wek, 2004), we examined the footprint coverage in the 5' UTR of these genes in more detail. In the case of *ATF4*, a markedly increased accumulation of footprints was observed at the most 5' Start-stop (St-st) element, specifically in eIF3d^{KD} and eIF3e^{KD}, while coverage of uORF1 decreased, and so did – modestly – also the basal level of uORF2 and *ATF4* (Figure 7E). This agrees well with our earlier observation that ribosomes are stalled at this St-st element (Wagner et al., 2020) and further suggests that both eIF3e and eIF3d are required to clear these St-st-trapped ribosomes. Regarding *MDM2*, footprint coverage was increased specifically for uORF1 in all three knock-downs, consistent with its several-fold stronger inhibitory role on MDM2 expression compared to uORF2 (Jin et al., 2003), which seems to be magnified in the absence of fully functional eIF3. Collectively, these results are in line with the well-established role of eIF3 in translation reinitiation (reviewed in (Valasek et al., 2017)). In addition, we found similarly accumulated footprints also at uORF1 and uORF2 of the RAF1 kinase, one of the downregulated components of the MAPK pathway (Supplementary Figure 10B).

Last but not least, eIF3d was shown to mediate mechanism of alternative cap-dependent translation initiation in conjunction with DAP5 (p97/NAT1) (Alard et al., 2023; de la Parra et al., 2018a; Volta et al., 2021) and, importantly, DAP5-dependent mRNAs also frequently contain uORFs (David et al., 2022). Consistent with this, the effects of depletion of DAP5 on the translatome were comparable to those observed in eIF3d-depleted cells (Supplementary Figure 11A - C); i.e., no changes in mRNA levels and the FP coverage moving in the same direction, either up or down. Since similar effects were also observed with eIF3e^{KD} and eIF3h^{KD}, it seems that the DAP5-dependent mechanism may rely upon not only on eIF3d but also on other eIF3 subunits.

Presence of uORFs, UTR length and GC content correlate with the change in translation efficiency

eIF3 is critically required for mRNA recruitment to the 40S ribosomal subunit (reviewed in (Valasek et al., 2017)) and several eIF3 subunits have been proposed to regulate translation of specific subsets of mRNAs (Lee et al., 2015; Lee et al., 2016). We therefore asked whether the changes in TE that were observed in the eIF3d, eIF3e or eIF3h knock-downs correlate with specific mRNA properties. Indeed, in all three knock-downs, the

change in TE was negatively correlated with the length of 5' and 3' UTR, and with the presence of uORFs in 5' UTR (Spearman correlation, $P < 1x10^{-45}$). Moreover, we found a significant positive Spearman correlation between TE changes and the GC content in the coding region (CDS) and 3' UTRs (Figure 8A).

To explore these correlations in more detail, we focused only on those mRNAs that are exclusively regulated at the translational level in each knock-down and therefore are more likely to contain distinct features that facilitate their translational regulation. We divided them into those with significantly changed TE (decreased and increased) and those with unchanged TE and searched for significant differences in the median values of the tested traits (Figure 8B - C). In accordance with the Spearman correlation, in eIF3d^{KD} and eIF3e^{KD}, mRNAs of downregulated DTEGs had longer 5' UTRs, while upregulated DTEGs possessed shorter 5' UTRs, when compared to mRNAs with unchanged TE. The same trend is seen for the 3' UTR length in eIF3e^{KD}, but with lower significance. In case of eIF3d^{KD}, only the downregulated DTEGs showed a significant change in 3' UTR length, but not DTEGs that were upregulated.

In terms of GC content, while we observed little significant difference in GC content in the 5' UTR of eIF3d^{KD} and eIF3e^{KD}, there was a highly significant difference in the CDS and 3' UTR of these knock-downs in both downregulated and upregulated DTEGs, indicating that mRNAs with increased TE tend to have more GC-rich 3' UTRs and, surprisingly, CDS and vice versa. For eIF3h^{KD}, we only observed differences of low significance due to the low number of DTEGs that were only translationally regulated (only 8 downregulated and 1 upregulated) (data not shown).

In summary, mRNAs with decreased TE in cells wherein eIF3d and eIF3e were depleted exhibited on average longer 5' and 3' UTRs and lower GC content in the CDS and 3' UTRs. In turn, mRNAs with increased TE have on average shorter 5' UTRs and a higher GC content in the CDS and 3' UTRs.

We next asked whether 5' UTRs of upregulated or downregulated DTEGs contain any specific sequence motifs or short upstream open reading frames (uORFs). We did not identify any specific sequence motif, but expectedly, the 5' UTRs of "downregulated translation only" DTEGs have a strong tendency to contain uORFs starting with AUG (Figure 8D - E). These findings suggest that the intact eIF3 complex is primarily required for translational control of subset of mRNAs containing short uORFs in their 5' UTR even under normal cellular conditions, like for example *MDM2*, *ATF4* or *RAF1*, which is in line with its role in translation reinitiation (Valasek et al., 2017), and further discussed below.

DISCUSSION

In this study, we interrogated the effects of altering composition of eIF3 by depleting three eIF3 subunits in HeLa cells, followed by RNA-Seq and Ribo-Seq to elucidate their role in translational regulation of specific mRNAs by differential expression analysis. We focused

on differential translation efficiency genes (DTEGs) and identified several distinct groups of DTEGs associated with individual eIF3 knock-downs.

Interestingly, while DTEGs identified in eIF3d^{KD} and eIF3e^{KD} largely overlapped, considerably more DTEGs were identified in eIF3d^{KD} then in eIF3e^{KD}, correlating well with the severity of the growth phenotype of both knock-downs, with the former being more detrimental despite not affecting eIF3 integrity (Wagner et al., 2016). The higher number of DTEGs identified in the same pathways in eIF3d^{KD} vs. eIF3e^{KD} could be explained by differences in eIF3d protein levels between the two knock-downs. Despite being markedly co-downregulated in eIF3e^{KD}, eIF3d levels were more dramatically reduced in eIF3d^{KD} vs. in eIF3e^{KD}. Furthermore, eIF3d is a peripheral subunit that binds to the head of the 40S subunit (mainly via the small ribosomal protein Rps16 (Herrmannova et al., 2020)) and is connected to the eIF3 octamer not only via eIF3e but also via the eIF3a and c subunits (Bochler et al., 2020). Therefore, we hypothesize that eIF3d may remain partially operational even in the absence of eIF3e, and therefore the more severe phenotype in eIF3d^{KD} is likely to stem from lower levels of the eIF3d protein compared to eIF3e^{KD}. Following this logic, phenotypes that are common to eIF3d^{KD} and eIF3e^{KD} are likely a consequence of reduction in eIF3d protein levels.

Perhaps the most intriguing finding is that eIF3d^{KD} and, to a large extent, also eIF3e^{KD} result in translational repression of a marked number of the MAPK pathway constituents, significantly reducing their protein levels, despite the apparent compensatory mechanisms that increase their transcription. Somewhat unexpectedly, despite the downregulation of a number of its components, eIF3d^{KD} and eIF3e^{KD} but also eIF3h^{KD} appear to activate MAPK pathway as evidenced by the elevated ERK1/2 and c-Jun phosphorylation. Notably, the eIF3d influence on the MAPK pathway was previously demonstrated in HTR-8/SVneo cells, where overexpression of eIF3d led to hypo-phosphorylation of MEK1 and ERK1/2, while downregulation had the opposite effect; however, no significant effect on the protein levels of its components was detected in this study (Li et al., 2021). Importantly, since the increased ERK1/2 phosphorylation was observed not only in eIF3d^{KD} and eIF3e^{KD} but also in eIF3h^{KD}, where expression of MAPK pathway proteins is unaffected, we conclude that activation of the MAPK pathway is a general consequence of compromised eIF3 function.

Expression of the transcription factor c-Jun is partially controlled by the MAPK pathway and, consistently, we found that it is strongly upregulated in all three knock-downs. Moreover, we observed that all three knockdowns activated c-Jun as evidenced by its increased nuclear translocation. Although *JUN* mRNA was previously shown to interact directly with eIF3 through a stable stem loop occurring in its 5' UTR, which positively stimulated its translation (Lee et al., 2015), in this study we observed the upregulation in the abundance of *JUN* mRNA, whereby the depletion of eIF3d, e, or h had no conspicuous effect on its translational efficiency. Recently, eIF3d was shown to bind to *JUN* mRNA with increased affinity during chronic ER stress, suggesting that

eIF3d-dependent translational regulation may be triggered by stress (Mukhopadhyay et al., 2023). Because c-Jun is a component of the AP1 transcription factor complex, wherein it either homodimerizes or heterodimerizes with other AP1 proteins, we examined the effects of eIF3 subunit depletion on mRNA, FP and TE trends of other AP1 family members. Similarly to c-Jun, only FOSL1 and ATF3 showed increased mRNA levels and FP counts with no net changes in TE, whereas other members of the JUN (JUNB and JUND) and FOS (FOS, FOSB, FOSL2) families remained unaltered. In addition, the ATF family members ATF2 and ATF4 were even downregulated (Supplementary Spreadsheet S2). Notwithstanding that our data suggest that impairment of eIF3 function may be compensated by the activation of the MAPK pathway, further research is required to unravel the full spectrum of changes associated with the activated MAPK pathway in eIF3-impaired cells.

Recently, Lin et al. carried out a similar analysis in MCF-10A cells downregulated for eIF3e (Lin et al., 2020). We cross-referenced our data with their eIF3e^{KD}-specific DTEGs (240 downregulated and 220 upregulated) and eIF3e-dependent mRNAs. They identified a set of 2683 eIF3e-dependent mRNAs encoding many proteins associated with mitochondrial and membrane functions that showed increased ribosome density between codons 25 and 75 in eIF3e^{KD}. Those mRNAs were therefore proposed to require eIF3e to recruit chaperons to promote their early elongation. However, we did not observe a similar phenomenon in our datasets. In metagene analysis, we did observe some accumulation of footprints at the beginning of the CDS, but this was present in all samples, including NT, whereby peaks were located around codon 20 downstream of the translation initiation sites (Supplementary Figure 12A). Nonetheless, “accumulation effect” observed by Lin et al., resulting from ribosome stalling or slower elongation/termination rates, could artificially increase FPs and TE without actually increasing translation and thus levels of the corresponding proteins. To ensure that this was not the case, we trimmed the first 225 nt (75 codons) from all mRNA’s CDSs, and repeated the differential expression analysis. When compared, the two DE analyses showed approximately 80% - 90% identical DTEGs and high correlation (Spearman correlation coefficient of eIF3d^{KD}: 0.924, eIF3e^{KD}: 0.925, eIF3h^{KD}: 0.834), suggesting that our DE analysis is not biased by ribosome accumulation in the first 75 codons and reflects true changes in translation efficiency. Interestingly, comparing our DTEGs with the Lin et al. data, we found a very significant overlap of 446 genes between the eIF3e-dependent mRNAs and our eIF3d^{KD} “all upregulated” dataset ($P < 1x10^{-53}$), while the overlap with eIF3e^{KD} “all upregulated” – 251 genes – was surprisingly smaller ($P < 1x10^{-24}$). Moreover, our KEGG enrichment analysis of eIF3e-dependent mRNAs from Lin et al. revealed the same top 2 KEGG pathways (data not shown) as in case of eIF3d^{KD} and eIF3e^{KD} “all upregulated” groups; i.e. Lysosome and Protein processing in ER (Figure 4A and Supplementary Figure 5A). Considering that eIF3d was co-depleted with eIF3e in the eIF3e^{KD} of Lin et al., it is conceivable that not eIF3e but the eIF3d subunit (or cooperatively

both subunits together) ensures loading of quality control factors to promote elongation of transmembrane proteins. In any case, resolving this issue will require further research.

Alternatively, based on our analysis, eIF3e may be primarily involved in controlling the balanced production of mature ribosomes, as its loss resulted in significant number of "unique upregulated" DTEGs with strong enrichment for the KEGG Ribosome and GO Translation and Ribosome biogenesis terms (Figure 4C and Supplementary Figure 5B). Focusing directly on RPs, nearly twice as many RPs with significantly altered TEs were identified in eIF3e^{KD} compared to eIF3d^{KD} (32 vs. 16) and a similar pattern was also evident at the FP level (91 vs. 64). However, despite this obvious difference, RPs were increased similarly in both eIF3d^{KD} and eIF3e^{KD} (Figure 4E). This discrepancy between our Ribo-Seq and Western blot results in eIF3e^{KD} *versus* eIF3d^{KD} (Figure 4D *vs.* 4E) might be explained by the enhanced stabilization of RPs by the previously described compensatory dosage mechanism at the protein level (Ishikawa, 2021). In particular, to preserve the stoichiometry of the ribosome when numerous RPs are translationally upregulated, the rest of the RPs would be protected from degradation. This speculation can be supported by the impact of all knock-downs on translation efficiency of different E3 ubiquitin ligases, as described for eIF3h^{KD} (Supplementary Table S5). Similar effect of increased RPs production was recently reported also for eIF3k^{KD} (Duan et al., 2023). Of note, eIF3e^{KD} also decreases protein levels of eIF3k and eIF3l and thus this RP-specific effect could be attributed to the loss of eIF3k. Increased RP production was however also observed in eIF3d^{KD}, where eIF3k is normally present, and was not observed in eIF3h^{KD}, where eIF3k and eIF3l are also co-depleted. Thus, although it now seems well-established that the eIF3 complex exerts control over RP production, the exact contribution of its individual subunits to this regulation awaits further analysis.

An important hint could be that all cytoplasmic RPs with increased TE in eIF3e^{KD} (and most of mitochondrial RPs) were upregulated solely at the translational level (their mRNA levels did not change), which may well correspond to the fact that RP mRNAs belong to the TOP mRNAs family. These mRNAs contain a polypyrimidine tract in their 5' UTR and were suggested to be regulated solely at the translational level in response to stress or unfavorable growth conditions through mTORC1 or PI3-kinase pathway (Cockman et al., 2020; Philippe et al., 2020; Stolovich et al., 2002). Besides RPs, this family also includes some translational initiation and elongation factors. Accordingly, we found that TOP transcripts were significantly translationally activated in eIF3d^{KD} and eIF3e^{KD} (Figure 5A - C), suggesting a role of eIF3e and eIF3d in repressing translation of TOP mRNAs under normal cellular conditions. Interestingly, since mTOR-activated translation of non-TOP transcripts was predominantly translationally offset (buffered) in eIF3d^{KD} and eIF3e^{KD} cells (Supplementary Figure 6A - C), it appears that both effects are independent of each other; i.e., mTOR does not generally operate *via* eIF3 and eIF3 does not require mTOR activation to fine tune RP production. It is also noteworthy that upregulation of cytosolic ribosomal proteins has previously been reported in association

with the eIF3m downregulation – albeit only at transcriptional level (Smekalova et al., 2020), or with downregulation of eEF2 (Gerashchenko et al., 2020). Furthermore, since one of the identified regulators – presumably suppressor – of 5' TOP mRNAs translation is LARP1 (Berman et al., 2021), we were wondering whether its steady state levels differed in our knock-downs, but found that the LARP1 protein production was unchanged as the FP count was not altered (Supplementary Spreadsheet S2).

In addition, as we were unable to find any specific sequence motif in the 5' UTR's of the mRNAs whose TE was affected in eIF3 subunit-depleted cells, we cross-referenced our eIF3d^{KD} "all" and eIF3e^{KD} "all" groups with transcripts that physically interact with eIF3 as reported by (Lee et al., 2015). We found that out of the 402 transcripts with a putative eIF3 binding sites in their 5' UTRs, 92 and 65 had significantly altered TE in the eIF3d^{KD} and eIF3e^{KD}, respectively (51 were common for both eIF3d^{KD} and eIF3e^{KD}) (Supplementary Figure 12B). This notable overlap involving for example MAPK1 gene further underscores the robustness of our screening approach.

Among the few downregulated DTEGs in eIF3h^{KD}, we found *ATF4* and *MDM2* mRNAs, whose translation is tightly regulated by the presence of uORFs in their 5' UTRs in response to specific stress conditions (Akulich et al., 2019; Dey et al., 2010; Jin et al., 2003). Here, we showed that these mRNAs were translationally downregulated in our knock-downs under non-stress conditions and, accordingly, their most 5' short uORFs (or St-st in the case of *ATF4*) accumulated FPs, most probably slowing down the flow of ribosomes downstream. The fact that transcripts of these genes contain uORFs in their 5' UTRs also correlates well with our finding that 5' UTRs of "downregulated translation only" DTEGs have a strong tendency to contain AUG-initiated uORFs (Figure 8D - E). Noteworthy, the impaired *ATF4* induction in our eIF3 knock-downs under ER stress (Figure 7D), was reported before also for knock-downs of eIF3a, eIF3c, eIF3d, eIF3g, but not eIF3l (Guan et al., 2017). Moreover, eIF3h and specifically modified eIF3a have been directly shown to modulate resumption of scanning from *ATF4*'s uORF1 for efficient reinitiation downstream; i.e. one of the key steps in the *ATF4* translational control (Hronova et al., 2017; Shu et al., 2022). Therefore, we propose that the intact eIF3 complex is required for stimulation of reinitiation on uORF-containing mRNAs, such as *ATF4* and *MDM2* to ensure their efficient translation on demand. Interestingly, the impact on translation of *MDM2* mRNA could indicate that intact eIF3 also contributes to the metabolism the key tumor suppressor p53 (Marine and Lozano, 2010), which is the focus of our further research.

Among a few upregulated DTEGs in eIF3h^{KD}, we noticed PRRC2A, which was significantly upregulated in all three knock-downs and was recently identified by the Teleman's group as a protein interacting with the translational machinery, including eIF3. Interestingly, they found that PRRC2 proteins affected translation initiation by promoting leaky scanning (Bohlen et al., 2023) and the triple knock-down of all PRRC2 proteins (PRRC2A, PRRC2B, PRRC2C) specifically decreased translation efficiency of mRNAs

harboring uORFs in their 5' UTRs, including *ATF4* and *RAF1* studied also here, similar to our eIF3 knock-downs. They concluded that uORFs are a key element determining PRRC2-dependence. Thus, we speculate that by increased expression of PRRC2A (and also PRRC2B and PRRC2C in eIF3d^{KD} and eIF3e^{KD}), cells attempt to compensate for ineffective translation of mRNAs with short uORFs, which often encode regulatory proteins. Intriguingly, all PRRC2 proteins themselves have a highly translated overlapping-uORF in their 5' UTR, suggesting that they might be a subject to an autoregulatory mechanism.

Although our results presented here and summarized in Figure 8F are limited to HeLa cells and future work is required to confirm their universal validity in other cells and tissues, growing evidence suggests that eIF3 plays a critical role in translational regulation of specific mRNAs encoding regulatory proteins, very often making use of uORFs and/or specific secondary structures in their 5' UTRs. Herein, we demonstrate that the alterations in the eIF3 subunit stoichiometry and/or eIF3 subcomplexes have distinct effects on the translatome. A great number of these proteins has been implicated in oncogenic signaling and tumor progression, and therefore many of them are considered actionable target for drug development. Since malignant cells exhibit augmented activity of many components of the translation machinery and are inherently believed to become "addicted" to elevated protein synthesis (Ruggero, 2013; Silvera et al., 2010), it is increasingly apparent that targeting directly general components of the canonical translational machinery, such as eIF3, which acts upstream of effector proteins directly involved in tumorigenesis, may hold promise for overcoming the major obstacle associated with intratumor heterogeneity.

ACKNOWLEDGMENTS

We are thankful to Olga Krýdová for technical and administrative assistance and to all lab members for fruitful discussions. We are also thankful to Jonathan Bohlen for sharing and discussing results of PRRC2 proteins downregulation. This work was supported by a Grant of Excellence in Basic Research (EXPRO 2019) provided by the Czech Science Foundation (19-25821X), the Praemium Academiae grant provided by the Czech Academy of Sciences, and CZ.02.01.01/00/22_008/0004575 RNA for therapy by ERDF and MEYS (all to L.S.V.), Czech Science Foundation grant 19-08013S (to T.V), ELIXIR CZ research infrastructure project (MEYS Grant No: LM2023055) including access to computing and storage facilities, by National Institute for Cancer Research (Programme EXCELES, ID Project No. LX22NPO5102) funded by the European Union - Next Generation EU (to J.B.) and by Fonds de Recherche du Québec – Santé (FRQS) Senior Investigator award (awarded to I.T.).

AUTHORS CONTRIBUTIONS

A.H. and L.S.V. conceived and designed the project.

A.H., J.J., K.P., F.K., T.V., K.W. and M.P.M. carried out all experiments and analyzed the data.
A.H., J.J. and L.S.V. interpreted results and wrote the paper with input from K.P., F.K., T.V., J.B., M.P.M., K.W., I.T. and S.W.

DECLARATION OF INTEREST

The authors declare no competing interests.

FIGURE LEGENDS

Figure 1. **Schematic models of the core of MAPK/ERK pathway and human eIF3 complex.** (A) The ERK pathway activation by growth factors and receptor tyrosine kinases (RTKs). RTKs signal through GRB2-Sos and Ras to activate Raf-MEK-ERK signaling cascade. Active ERK phosphorylates numerous substrates, both nuclear and cytoplasmic, to affect gene transcription, protein translation, cell growth, proliferation and survival. Both RTKs and Ras also activate PI3K-AKT pathway that affect cell survival and growth. Conventional PAKs (PAK1-3) phosphorylate c-Raf and contribute to its activation. Created with Biorender.com. (B) eIF3 subunits forming the PCI/MPN octamer are indicated by the grey background. The rectangle marks the seven α-helices involved in formation of the 7-helix bundle. The Yeast-Like Core (YLC) comprising the eIF3 subunits a, b, g and i is depicted, and so is the eIF3-associated factor eIF3j. Arrows indicate subunits targeted by siRNA and subjected to Ribo-Seq in this study; eIF3 subcomplexes generated in individual knock-downs are boxed (adapted from (Wagner et al., 2016)).

Figure 2. **Quality control of eIF3e, d, and h knock-downs and the Ribo-Seq data**
(A) mRNA levels of the selected downregulated eIF3 subunits were significantly decreased as assessed by quantitative PCR for all replicates. Plot represents the result of all replicates used for RNA-Seq and Ribo-Seq library preparations ± SD. The ddCq value displays the threshold cycle normalized to the reference gene *ALAS1* and to control cells transfected with non-targeting siRNA (NT). The ddCq values are in log2 scale. A ddCq of 0 indicates no change to NT siRNA control; ddCq = 4 indicates a drop to 6.25% (16 fold) compared to NT siRNA control. (B) Downregulation of selected eIF3 subunits targeted by siRNA was determined by Western blotting with GAPDH used as a loading control and antibodies listed in Supplementary Table S3. (C) All Ribo-Seq libraries show typical 3nt periodicity in the CDS. Metagene plots of footprint (FP) length versus 5' end position relative to the first nucleotide (position 0) of start (left) or stop codons (right). The color scale represents FP count as indicated on the right and is plotted in log scale. The labels at the color bar are given in linear scale. Heatmaps are shown for one exemplary replicate from each sample.

Figure 3. **DTEGs identified in eIF3d^{KD}, eIF3e^{KD} and eIF3h^{KD} largely overlap.** (A) Principal component analysis of read count per gene of the RNA-Seq and Ribo-Seq libraries. (B - D) Volcano plots of significant ($P_{adjusted} < 0.05$) DTEGs in individual knock-downs: eIF3d^{KD} (B), eIF3e^{KD} (C) and eIF3h^{KD} (D). The volcano plots show the Log2 fold-change of TE (x-axis) *versus* the significance -Log10 p-adjusted value (y-axis). Genes without significant p-adjusted value are plotted in grey, downregulated DTEGs are plotted in blue and upregulated DTEGs in orange. For each plot, the top 10 most significant DTEGs are labeled with gene names. The Volcano plots were generated using modified script from Galaxy (Blankenberg et al., 2014). (E - G) Venn diagrams depicting the overlap in all DTEGs (E), in upregulated DTEGs (F), and in downregulated DTEGs (G) among eIF3d^{KD}, eIF3e^{KD} and eIF3h^{KD}. Based on the overlaps, DTEGs were divided in several subgroups for further analysis: eIF3d^{KD} "all", eIF3d^{KD} "unique", eIF3e^{KD} "all", eIF3e^{KD} "unique", eIF3d^{KD}/eIF3e^{KD} "common" and eIF3h^{KD} "all".

Figure 4. **KEGG pathway enrichment analysis of the eIF3d^{KD}- and eIF3e^{KD}-associated upregulated DTEGs reveals upregulation of ribosomal proteins.** (A) Venn diagram of the 10 most significantly enriched KEGG pathways for eIF3d^{KD} "all" and eIF3e^{KD} "all" groups of upregulated DTEGs, highlighting that most of the pathways are common to both knock-downs. Lysosome and Protein processing in ER are highlighted in bold. The complete results of the KEGG enrichment analysis with corresponding *p*-values can be found in Supplementary Figure 5A. (B) Venn diagram as in A but displaying eIF3d^{KD} "translation only" and eIF3e^{KD} "translation only" groups of the upregulated DTEGs. (C) The bar chart shows the top 10 enriched KEGG terms for eIF3e^{KD} "unique" upregulated DTEGs. Orange bars correspond to terms with significant *p*-values (< 0.05), grey bars correspond to terms with not significant *p*-values (> 0.05). The *p*-values were calculated by Enrichr gene set search engine. (D) The list of genes pre-selected for western blot analysis and a heatmap showing their respective log2 fold-change values from differential expression analysis of FP, TE and mRNA in eIF3e^{KD} and eIF3d^{KD}. Positive values indicating significant upregulation are in shades of orange. NS = not significant p-adjusted value. (E) Western blot analysis of selected ribosomal proteins performed in the indicated knock-downs and the NT control. GAPDH was used as a loading control. This experiment was repeated 3 times with similar results.

Figure 5. **Loss of eIF3 subunits leads to translational activation of mRNAs with 5'UTR TOP motifs.**
(A-C) Scatterplots from translatome analysis of eIF3d^{KD} (A), eIF3e^{KD} (B), and eIF3h^{KD} (C) with the location of transcripts harboring 5' UTR TOP motifs (Philippe et al., 2020) colored (left panels). Middle and right panels show the empirical cumulative distribution functions of $\log_2$ fold changes in FP and total mRNA for the transcripts with TOP motifs. The background constituting all other transcripts are shown as grey curves. Significant

differences between the distributions were identified using the Wilcoxon rank-sum test. Differences between the distributions at each quantile are indicated. Shift to the right indicates increased expression, while shift to the left indicates decreased expression.

Figure 6. **KEGG pathway enrichment analysis of the eIF3d^{KD}- and eIF3e^{KD}-associated downregulated DTEGs reveals downregulation of MAPK signaling pathway components.** (A) Venn diagram of the 10 most significantly enriched KEGG pathways for eIF3d^{KD} "all" and eIF3e^{KD} "all" groups of downregulated DTEGs, highlighting that most of the pathways are common to both knock-downs. The MAPK signaling pathway is highlighted in bold. The complete results of the KEGG enrichment analysis with corresponding *p*-values can be found in Supplementary Figure 7A. (B) The list of genes pre-selected for western blot analysis and a heatmap showing their respective log2 fold-change values from differential expression analysis of FP, TE and mRNA in eIF3d^{KD}. Negative values indicating a significant downregulation are in shades of blue, while positive values showing significant upregulation are in shades of orange. NS = not significant p-adjusted value. (C) Western blot analysis of selected proteins constituting the MAPK pathway performed in the indicated knock-downs and the NT control. GAPDH was used as a loading control. This experiment was repeated 3 times with similar results. (D) Western blot analysis of the phosphorylation status of the ERK1/2 proteins (left) and its relative quantification (right), one-sample t-test was used for statistical evaluation, ** = P <0.01, n=2. (E) Western blot analysis of the phosphorylation status of the c-Jun transcription factor in cytoplasmatic and nuclear fractions in the indicated knock-downs and the NT control. The protein loading was 50ug of total protein for cytoplasmatic lysate and 20ug of total protein for nuclear lysate, as indicated. GAPDH was used as a loading control. This experiment was repeated 3 times with similar results.

Figure 7. **KEGG pathway and GO enrichment analysis of the eIF3h^{KD}-associated DTEGs reveals downregulation of proto-oncogene MDM2 and a defective stress-induced upregulation of ATF4.** (A) The bar chart shows the top 10 enriched KEGG terms for eIF3h^{KD} "all downregulated" DTEGs. Blue bars correspond to terms with significant *p*-values (< 0.05), grey bars correspond to terms with not significant *p*-values (> 0.05). The *p*-values were calculated by Enrichr gene set search engine. (B) The bar chart shows the top 10 enriched GO Biological Process terms for eIF3h^{KD} "all downregulated" DTEGs. Blue bars correspond to terms with significant *p*-values (< 0.05). The *p*-values were calculated by Enrichr gene set search engine. PCP; protein catabolic process. (C) Western blot analysis of the MDM2 expression preformed in the indicated knock-downs and NT control. GAPDH was used as a loading control. (D) Western blot analysis of the stress-induced upregulation of ATF4 expression performed in the indicated knock-downs and NT control. Before harvesting, cells were incubated for 3 hours with 1mM Thapsigargin to induce ER stress or with DMSO as a stress-free control. GAPDH

was used as a loading control. (E) Normalized ribosomal footprint coverage along the *ATF4* mRNA (first 450 nucleotides). Schematic with regulatory elements is shown at the bottom. Average of all three replicates is shown. Footprint coverage was normalized to all footprints mapping to the *ATF4* mRNA. (F) Same as in (E) only for *MDM2* mRNA.

Figure 8. **Differential TE transcripts in eIF3d^{KD} and eIF3e^{KD} show negative correlation with the UTR length and uORF content while they positively correlate with GC content of their 3' UTRs and coding sequences (CDS).** (A) Bar plot showing the Spearman correlation between the observed ΔTE values for all genes with assigned adjusted *p*-values in each knock-down and different mRNA features (5' and 3' UTR length or GC content, uORF content in 5' UTR). *** = P < 10^{-20}, ** = P < 10^{-10}, * = P < 0.005. (B-C) Box and whisker plots comparing UTR lengths or GC content (in UTRs or CDS) among mRNAs with TE significantly increased (red, upregulated), decreased (blue, downregulated), or unchanged (white) in eIF3d^{KD} (B) and eIF3e^{KD} (C); *** = Padj < 10^{-10} , ** = Padj < 10^{-5}, * = Padj < 0.05, color indicates comparison set. (D) Same as in (B-C) but for the number of AUG-initiated uORFs in 5' UTRs in the eIF3d, eIF3e and eIF3h knock-downs. Outliers are not shown for better clarity. (E) Histogram of the frequency of AUG-initiated uORFs per 5' UTR in all transcripts listed in the uORFdb database that were assigned a *p*-value in this study (n=11450), for downregulated translation only DTEGs in eIF3d^{KD} (n=1027) and for downregulated translation only DTEGs in eIF3e^{KD} (n=618). (F) Venn diagram summarizing the main results of this study. Groups of significant DTEGs identified in given knock-downs (encircled – color-coded) are indicated by a blue arrow for downregulated or an orange arrow for upregulated. Results confirmed by western blotting are shown in bold. Ribosomal proteins were placed on the borderline between eIF3d^{KD} and eIF3e^{KD} because they were identified as eIF3e^{KD} "unique upregulated" DTEGs, but their protein levels were elevated in both eIF3e^{KD} and eIF3d^{KD}, as shown by western blotting. The "MAPK/ERK signaling" is shown in bold italics because it is an independent phenomenon that could be detected only by western blotting.

SUPPLEMENTAL INFORMATION

Supplemental Information can be found online at ….

DATA AVAILABILITY

The datasets generated during this study were deposited in the GEO database with the following accession number: GSE216967. All custom programs source code are published at https://github.com/cas-bioinf/RibosomeProfiling.

REFERENCES

Akulich, K.A., Sinitcyn, P.G., Makeeva, D.S., Andreev, D.E., Terenin, I.M., Anisimova, A.S., Shatsky, I.N., and Dmitriev, S.E. (2019). A novel uORF-based regulatory mechanism controls translation of the human MDM2 and eIF2D mRNAs during stress. Biochimie *157*, 92-101.
Alard, A., Katsara, O., Rios-Fuller, T., Parra, C., Ozerdem, U., Ernlund, A., and Schneider, R.J. (2023). Breast cancer cell mesenchymal transition and metastasis directed by DAP5/eIF3d-mediated selective mRNA translation. Cell Rep *42*, 112646.
Anders, S., Pyl, P.T., and Huber, W. (2015). HTSeq--a Python framework to work with high-throughput sequencing data. Bioinformatics *31*, 166-169.
Andrews, S. (2010). FastQC: A quality control tool for high throughput sequence data. .
Ashburner, M., Ball, C.A., Blake, J.A., Botstein, D., Butler, H., Cherry, J.M., Davis, A.P., Dolinski, K., Dwight, S.S., Eppig, J.T.*, et al.* (2000). Gene ontology: tool for the unification of biology. The Gene Ontology Consortium. Nat Genet *25*, 25-29.
Berman, A.J., Thoreen, C.C., Dedeic, Z., Chettle, J., Roux, P.P., and Blagden, S.P. (2021). Controversies around the function of LARP1. RNA Biol *18*, 207-217.
Beznosková, P., Cuchalová, L., Wagner, S., Shoemaker, C.J., Gunišová, S., Von der Haar, T., and Valášek, L.S. (2013). Translation initiation factors eIF3 and HCR1 control translation termination and stop codon read-through in yeast cells. PLoS Genet *9*, e1003962.
Beznosková, P., Wagner, S., Jansen, M.E., von der Haar, T., and Valášek, L.S. (2015). Translation initiation factor eIF3 promotes programmed stop codon readthrough. Nucleic Acids Res *43*, 5099-5111.
Bhat, M., Robichaud, N., Hulea, L., Sonenberg, N., Pelletier, J., and Topisirovic, I. (2015). Targeting the translation machinery in cancer. Nat Rev Drug Discov *14*, 261-278.
Blankenberg, D., Von Kuster, G., Bouvier, E., Baker, D., Afgan, E., Stoler, N., Galaxy, T., Taylor, J., and Nekrutenko, A. (2014). Dissemination of scientific software with Galaxy ToolShed. Genome Biol *15*, 403.
Bochler, A., Querido, J.B., Prilepskaja, T., Soufari, H., Simonetti, A., Del Cistia, M.L., Kuhn, L., Ribeiro, A.R., Valasek, L.S., and Hashem, Y. (2020). Structural Differences in Translation Initiation between Pathogenic Trypanosomatids and Their Mammalian Hosts. Cell Rep *33*, 108534.
Bohlen, J., Roiuk, M., Neff, M., and Teleman, A.A. (2023). PRRC2 proteins impact translation initiation by promoting leaky scanning. Nucleic Acids Res *51*, 3391-3409.
Brito Querido, J., Sokabe, M., Kraatz, S., Gordiyenko, Y., Skehel, J.M., Fraser, C.S., and Ramakrishnan, V. (2020). Structure of a human 48S translational initiation complex. Science *369*, 1220-1227.
Buxade, M., Parra-Palau, J.L., and Proud, C.G. (2008). The Mnks: MAP kinase-interacting kinases (MAP kinase signal-integrating kinases). Front Biosci *13*, 5359-5373.
Calviello, L., WSydow, D., Harnett, D., and Ohler, U. (2019). Ribo-seQC: comprehensive analysis of cytoplasmic and organellar ribosome profiling data. bioRxiv 601468.
Cargnello, M., and Roux, P.P. (2011). Activation and function of the MAPKs and their substrates, the MAPK-activated protein kinases. Microbiol Mol Biol Rev *75*, 50-83.
Carriere, A., Ray, H., Blenis, J., and Roux, P.P. (2008). The RSK factors of activating the Ras/MAPK signaling cascade. Front Biosci *13*, 4258-4275.
Cate, J.H. (2017). Human eIF3: from 'blobology' to biological insight. Philos Trans R Soc Lond B Biol Sci *372*.

Chan, P.P., and Lowe, T.M. (2016). GtRNAdb 2.0: an expanded database of transfer RNA genes identified in complete and draft genomes. Nucleic Acids Res *44*, D184-189.
Chothani, S., Adami, E., Ouyang, J.F., Viswanathan, S., Hubner, N., Cook, S.A., Schafer, S., and Rackham, O.J.L. (2019). deltaTE: Detection of Translationally Regulated Genes by Integrative Analysis of Ribo-seq and RNA-seq Data. Curr Protoc Mol Biol *129*, e108.
Cockman, E., Anderson, P., and Ivanov, P. (2020). TOP mRNPs: Molecular Mechanisms and Principles of Regulation. Biomolecules *10*.
Colak, S., and Ten Dijke, P. (2017). Targeting TGF-beta Signaling in Cancer. Trends Cancer *3*, 56-71.
Cooper, J., and Giancotti, F.G. (2019). Integrin Signaling in Cancer: Mechanotransduction, Stemness, Epithelial Plasticity, and Therapeutic Resistance. Cancer Cell *35*, 347-367.
Danecek, P., Bonfield, J.K., Liddle, J., Marshall, J., Ohan, V., Pollard, M.O., Whitwham, A., Keane, T., McCarthy, S.A., Davies, R.M.*, et al.* (2021). Twelve years of SAMtools and BCFtools. Gigascience *10*.
David, M., Olender, T., Mizrahi, O., Weingarten-Gabbay, S., Friedlander, G., Meril, S., Goldberg, N., Savidor, A., Levin, Y., Salomon, V.*, et al.* (2022). DAP5 drives translation of specific mRNA targets with upstream ORFs in human embryonic stem cells. RNA *28*, 1325-1336.
De Benedetti, A., and Harris, A.L. (1999). eIF4E expression in tumors: its possible role in progression of malignancies. Int J Biochem Cell Biol *31*, 59-72.
de la Parra, C., Ernlund, A., Alard, A., Ruggles, K., Ueberheide, B., and Schneider, R.J. (2018a). A widespread alternate form of cap-dependent mRNA translation initiation. Nat Commun *9*, 3068.
de la Parra, C., Walters, B.A., Geter, P., and Schneider, R.J. (2018b). Translation initiation factors and their relevance in cancer. Curr Opin Genet Dev *48*, 82-88.
des Georges, A., Dhote, V., Kuhn, L., Hellen, C.U., Pestova, T.V., Frank, J., and Hashem, Y. (2015). Structure of mammalian eIF3 in the context of the 43S preinitiation complex. Nature *525*, 491-495.
Dey, S., Baird, T.D., Zhou, D., Palam, L.R., Spandau, D.F., and Wek, R.C. (2010). Both transcriptional regulation and translational control of ATF4 are central to the integrated stress response. J Biol Chem *285*, 33165-33174.
Dhillon, A.S., Hagan, S., Rath, O., and Kolch, W. (2007). MAP kinase signalling pathways in cancer. Oncogene *26*, 3279-3290.
Dobin, A., Davis, C.A., Schlesinger, F., Drenkow, J., Zaleski, C., Jha, S., Batut, P., Chaisson, M., and Gingeras, T.R. (2013). STAR: ultrafast universal RNA-seq aligner. Bioinformatics *29*, 15-21.
Duan, H., Zhang, S., Zarai, Y., Ollinger, R., Wu, Y., Sun, L., Hu, C., He, Y., Tian, G., Rad, R.*, et al.* (2023). eIF3 mRNA selectivity profiling reveals eIF3k as a cancer-relevant regulator of ribosome content. EMBO J, e112362.
Durinck, S., Spellman, P.T., Birney, E., and Huber, W. (2009). Mapping identifiers for the integration of genomic datasets with the R/Bioconductor package biomaRt. Nat Protoc *4*, 1184-1191.
Fukunaga, R., and Hunter, T. (1997). MNK1, a new MAP kinase-activated protein kinase, isolated by a novel expression screening method for identifying protein kinase substrates. EMBO J *16*, 1921-1933.

Furic, L., Rong, L., Larsson, O., Koumakpayi, I.H., Yoshida, K., Brueschke, A., Petroulakis, E., Robichaud, N., Pollak, M., Gaboury, L.A.*, et al.* (2010). eIF4E phosphorylation promotes tumorigenesis and is associated with prostate cancer progression. Proc Natl Acad Sci U S A *107*, 14134-14139.
Gandin, V., Masvidal, L., Cargnello, M., Gyenis, L., McLaughlan, S., Cai, Y., Tenkerian, C., Morita, M., Balanathan, P., Jean-Jean, O.*, et al.* (2016). mTORC1 and CK2 coordinate ternary and eIF4F complex assembly. Nat Commun *7*, 11127.
Ge, S.X., Jung, D., and Yao, R. (2020). ShinyGO: a graphical gene-set enrichment tool for animals and plants. Bioinformatics *36*, 2628-2629.
Gene Ontology, C. (2021). The Gene Ontology resource: enriching a GOld mine. Nucleic Acids Res *49*, D325-D334.
Gerashchenko, M.V., Nesterchuk, M.V., Smekalova, E.M., Paulo, J.A., Kowalski, P.S., Akulich, K.A., Bogorad, R., Dmitriev, S.E., Gygi, S., Zatsepin, T.*, et al.* (2020). Translation elongation factor 2 depletion by siRNA in mouse liver leads to mTOR-independent translational upregulation of ribosomal protein genes. Sci Rep *10*, 15473.
Gomes-Duarte, A., Lacerda, R., Menezes, J., and Romao, L. (2018). eIF3: a factor for human health and disease. RNA Biol *15*, 26-34.
Guan, B.J., van Hoef, V., Jobava, R., Elroy-Stein, O., Valasek, L.S., Cargnello, M., Gao, X.H., Krokowski, D., Merrick, W.C., Kimball, S.R.*, et al.* (2017). A Unique ISR Program Determines Cellular Responses to Chronic Stress. Mol Cell *68*, 885-900 e886.
Harding, H.P., Novoa, I., Zhang, Y., Zeng, H., Wek, R., Schapira, M., and Ron, D. (2000). Regulated translation initiation controls stress-induced gene expression in mammalian cells. Mol Cell *6*, 1099-1108.
Heberle, H., Meirelles, G.V., da Silva, F.R., Telles, G.P., and Minghim, R. (2015). InteractiVenn: a web-based tool for the analysis of sets through Venn diagrams. BMC Bioinformatics *16*, 169.
Herrmannova, A., Prilepskaja, T., Wagner, S., Sikrova, D., Zeman, J., Poncova, K., and Valasek, L.S. (2020). Adapted formaldehyde gradient cross-linking protocol implicates human eIF3d and eIF3c, k and l subunits in the 43S and 48S pre-initiation complex assembly, respectively. Nucleic Acids Res *48*, 1969-1984.
Hershey, J.W. (2015). The role of eIF3 and its individual subunits in cancer. Biochim Biophys Acta *1849*, 792-800.
Hinnebusch, A.G. (2017). Structural Insights into the Mechanism of Scanning and Start Codon Recognition in Eukaryotic Translation Initiation. Trends Biochem Sci *42*, 589-611.
Howe, K.L., Achuthan, P., Allen, J., Allen, J., Alvarez-Jarreta, J., Amode, M.R., Armean, I.M., Azov, A.G., Bennett, R., Bhai, J.*, et al.* (2021). Ensembl 2021. Nucleic Acids Res *49*, D884-D891.
Hronova, V., Mohammad, M.P., Wagner, S., Panek, J., Gunisova, S., Zeman, J., Poncova, K., and Valasek, L.S. (2017). Does eIF3 promote reinitiation after translation of short upstream ORFs also in mammalian cells? RNA biol, doi: 10.1080/15476286.15472017.11353863.
Ingolia, N.T., Brar, G.A., Rouskin, S., McGeachy, A.M., and Weissman, J.S. (2012). The ribosome profiling strategy for monitoring translation in vivo by deep sequencing of ribosome-protected mRNA fragments. Nat Protoc *7*, 1534-1550.
Ishikawa, K. (2021). Multilayered regulation of proteome stoichiometry. Curr Genet *67*, 883-890.

Jin, X., Turcott, E., Englehardt, S., Mize, G.J., and Morris, D.R. (2003). The two upstream open reading frames of oncogene mdm2 have different translational regulatory properties. J Biol Chem *278*, 25716-25721.
Juhling, F., Morl, M., Hartmann, R.K., Sprinzl, M., Stadler, P.F., and Putz, J. (2009). tRNAdb 2009: compilation of tRNA sequences and tRNA genes. Nucleic Acids Res *37*, D159-162.
Kandoth, C., McLellan, M.D., Vandin, F., Ye, K., Niu, B., Lu, C., Xie, M., Zhang, Q., McMichael, J.F., Wyczalkowski, M.A.*, et al.* (2013). Mutational landscape and significance across 12 major cancer types. Nature *502*, 333-339.
Kanehisa, M., and Sato, Y. (2020). KEGG Mapper for inferring cellular functions from protein sequences. Protein Sci *29*, 28-35.
Kanehisa, M., Sato, Y., and Kawashima, M. (2022). KEGG mapping tools for uncovering hidden features in biological data. Protein Sci *31*, 47-53.
Karampelias, C., Watt, K., Mattsson, C.L., Ruiz, A.F., Rezanejad, H., Mi, J., Liu, X., Chu, L., Locasale, J.W., Korbutt, G.S.*, et al.* (2022). MNK2 deficiency potentiates beta-cell regeneration via translational regulation. Nat Chem Biol *18*, 942-953.
King, A.J., Sun, H., Diaz, B., Barnard, D., Miao, W., Bagrodia, S., and Marshall, M.S. (1998). The protein kinase Pak3 positively regulates Raf-1 activity through phosphorylation of serine 338. Nature *396*, 180-183.
Kovalski, J.R., Kuzuoglu-Ozturk, D., and Ruggero, D. (2022). Protein synthesis control in cancer: selectivity and therapeutic targeting. EMBO J *41*, e109823.
Kuleshov, M.V., Jones, M.R., Rouillard, A.D., Fernandez, N.F., Duan, Q., Wang, Z., Koplev, S., Jenkins, S.L., Jagodnik, K.M., Lachmann, A.*, et al.* (2016). Enrichr: a comprehensive gene set enrichment analysis web server 2016 update. Nucleic Acids Res *44*, W90-97.
Kusnadi, E.P., Timpone, C., Topisirovic, I., Larsson, O., and Furic, L. (2022). Regulation of gene expression via translational buffering. Biochim Biophys Acta Mol Cell Res *1869*, 119140.
Langmead, B., and Salzberg, S.L. (2012). Fast gapped-read alignment with Bowtie 2. Nat Methods *9*, 357-359.
Lauria, F., Tebaldi, T., Bernabo, P., Groen, E.J.N., Gillingwater, T.H., and Viero, G. (2018). riboWaltz: Optimization of ribosome P-site positioning in ribosome profiling data. PLoS Comput Biol *14*, e1006169.
Lavoie, H., Gagnon, J., and Therrien, M. (2020). ERK signalling: a master regulator of cell behaviour, life and fate. Nat Rev Mol Cell Biol *21*, 607-632.
Lazaris-Karatzas, A., Montine, K.S., and Sonenberg, N. (1990). Malignant transformation by a eukaryotic initiation factor subunit that binds to mRNA 5' cap. Nature *345*, 544-547.
Lee, A.S., Kranzusch, P.J., and Cate, J.H. (2015). eIF3 targets cell-proliferation messenger RNAs for translational activation or repression. Nature *522*, 111-114.
Lee, A.S., Kranzusch, P.J., Doudna, J.A., and Cate, J.H. (2016). eIF3d is an mRNA cap-binding protein that is required for specialized translation initiation. Nature *536*, 96-99.
Leppa, S., Saffrich, R., Ansorge, W., and Bohmann, D. (1998). Differential regulation of c-Jun by ERK and JNK during PC12 cell differentiation. EMBO J *17*, 4404-4413.
Li, X., Wang, Z., Liu, G., and Guo, J. (2021). EIF3D promotes the progression of preeclampsia by inhibiting of MAPK/ERK1/2 pathway. Reprod Toxicol *105*, 166-174.

Lin, Y., Li, F., Huang, L., Polte, C., Duan, H., Fang, J., Sun, L., Xing, X., Tian, G., Cheng, Y.*, et al.* (2020). eIF3 Associates with 80S Ribosomes to Promote Translation Elongation, Mitochondrial Homeostasis, and Muscle Health. Mol Cell *79*, 575-587 e577.
Lindqvist, L.M., Tandoc, K., Topisirovic, I., and Furic, L. (2018). Cross-talk between protein synthesis, energy metabolism and autophagy in cancer. Curr Opin Genet Dev *48*, 104-111.
Liu, T., Zhang, L., Joo, D., and Sun, S.C. (2017). NF-kappaB signaling in inflammation. Signal Transduct Target Ther *2*, 17023-.
Llacer, J.L., Hussain, T., Dong, J., Villamayor, L., Gordiyenko, Y., and Hinnebusch, A.G. (2021). Large-scale movement of eIF3 domains during translation initiation modulate start codon selection. Nucleic Acids Res *49*, 11491-11511.
Llácer, J.L., Hussain, T., Gordiyenko, Y., Lorsch, J.R., Hinnebusch, A.G., and Ramakrishnan, V. (2018). The beta propellers of eIF3b and eIF3i relocate together to the ribosomal intersubunit interface during translation initiation. bioRxiv, 453688.
Love, M.I., Huber, W., and Anders, S. (2014). Moderated estimation of fold change and dispersion for RNA-seq data with DESeq2. Genome Biol *15*, 550.
Lu, P.D., Harding, H.P., and Ron, D. (2004). Translation reinitiation at alternative open reading frames regulates gene expression in an integrated stress response. J Cell Biol *167*, 27-33.
Manske, F., Ogoniak, L., Jurgens, L., Grundmann, N., Makalowski, W., and Wethmar, K. (2023). The new uORFdb: integrating literature, sequence, and variation data in a central hub for uORF research. Nucleic Acids Res *51*, D328-D336.
Marine, J.C., and Lozano, G. (2010). Mdm2-mediated ubiquitylation: p53 and beyond. Cell Death Differ *17*, 93-102.
Martin, M. (2011). Cutadapt removes adapter sequences from high-throughput sequencing reads. EMBnetjournal *17*, 10-12.
Morales, J., Pujar, S., Loveland, J.E., Astashyn, A., Bennett, R., Berry, A., Cox, E., Davidson, C., Ermolaeva, O., Farrell, C.M.*, et al.* (2022). A joint NCBI and EMBL-EBI transcript set for clinical genomics and research. Nature *604*, 310-315.
Mukhopadhyay, S., Amodeo, M.E., and Lee, A.S.Y. (2023). eIF3d controls the persistent integrated stress response. Mol Cell *83*, 3303-3313 e3306.
Pakos-Zebrucka, K., Koryga, I., Mnich, K., Ljujic, M., Samali, A., and Gorman, A.M. (2016). The integrated stress response. EMBO Rep *17*, 1374-1395.
Pearce, S.F., Cipullo, M., Chung, B., Brierley, I., and Rorbach, J. (2021). Mitoribosome Profiling from Human Cell Culture: A High Resolution View of Mitochondrial Translation. Methods Mol Biol *2192*, 183-196.
Philippe, L., van den Elzen, A.M.G., Watson, M.J., and Thoreen, C.C. (2020). Global analysis of LARP1 translation targets reveals tunable and dynamic features of 5' TOP motifs. Proc Natl Acad Sci U S A *117*, 5319-5328.
Pisarev, A.V., Hellen, C.U.T., and Pestova, T.V. (2007). Recycling of Eukaryotic Posttermination Ribosomal Complexes. Cell *131*, 286–299.
Poncova, K., Wagner, S., Jansen, M.E., Beznoskova, P., Gunisova, S., Herrmannova, A., Zeman, J., Dong, J., and Valasek, L.S. (2019). uS3/Rps3 controls fidelity of translation termination and programmed stop codon readthrough in co-operation with eIF3. Nucleic Acids Res *47*, 11326-11343.

Pyronnet, S., Imataka, H., Gingras, A.C., Fukunaga, R., Hunter, T., and Sonenberg, N. (1999). Human eukaryotic translation initiation factor 4G (eIF4G) recruits Mnk1 to phosphorylate eIF4E. EMBO Journal *18*, 270-279.
Rayburn, E., Zhang, R., He, J., and Wang, H. (2005). MDM2 and human malignancies: expression, clinical pathology, prognostic markers, and implications for chemotherapy. Curr Cancer Drug Targets *5*, 27-41.
Robichaud, N., del Rincon, S.V., Huor, B., Alain, T., Petruccelli, L.A., Hearnden, J., Goncalves, C., Grotegut, S., Spruck, C.H., Furic, L.*, et al.* (2015). Phosphorylation of eIF4E promotes EMT and metastasis via translational control of SNAIL and MMP-3. Oncogene *34*, 2032-2042.
Robichaud, N., and Sonenberg, N. (2017). Translational control and the cancer cell response to stress. Curr Opin Cell Biol *45*, 102-109.
Robichaud, N., Sonenberg, N., Ruggero, D., and Schneider, R.J. (2019). Translational Control in Cancer. Cold Spring Harb Perspect Biol *11*.
Roux, P.P., Ballif, B.A., Anjum, R., Gygi, S.P., and Blenis, J. (2004). Tumor-promoting phorbol esters and activated Ras inactivate the tuberous sclerosis tumor suppressor complex via p90 ribosomal S6 kinase. Proc Natl Acad Sci U S A *101*, 13489-13494.
Roux, P.P., and Topisirovic, I. (2018). Signaling Pathways Involved in the Regulation of mRNA Translation. Mol Cell Biol *38*.
Ruggero, D. (2013). Translational control in cancer etiology. Cold Spring Harb Perspect Biol *5*.
Sayers, E.W., Bolton, E.E., Brister, J.R., Canese, K., Chan, J., Comeau, D.C., Connor, R., Funk, K., Kelly, C., Kim, S.*, et al.* (2022). Database resources of the national center for biotechnology information. Nucleic Acids Res *50*, D20-D26.
Scheper, G.C., van der Knaap, M.S., and Proud, C.G. (2007). Translation matters: protein synthesis defects in inherited disease. Nat Rev Genet *8*, 711-723.
She, R., Luo, J., and Weissman, J.S. (2023). Translational fidelity screens in mammalian cells reveal eIF3 and eIF4G2 as regulators of start codon selectivity. Nucleic Acids Res.
Shu, X.E., Mao, Y., Jia, L., and Qian, S.B. (2022). Dynamic eIF3a O-GlcNAcylation controls translation reinitiation during nutrient stress. Nat Chem Biol *18*, 134-141.
Shuda, M., Kondoh, N., Tanaka, K., Ryo, A., Wakatsuki, T., Hada, A., Goseki, N., Igari, T., Hatsuse, K., Aihara, T.*, et al.* (2000). Enhanced expression of translation factor mRNAs in hepatocellular carcinoma. Anticancer Res *20*, 2489-2494.
Silvera, D., Formenti, S.C., and Schneider, R.J. (2010). Translational control in cancer. Nat Rev Cancer *10*, 254-266.
Simonetti, A., Guca, E., Bochler, A., Kuhn, L., and Hashem, Y. (2020). Structural Insights into the Mammalian Late-Stage Initiation Complexes. Cell Rep *31*, 107497.
Smekalova, E.M., Gerashchenko, M.V., O'Connor, P.B.F., Whittaker, C.A., Kauffman, K.J., Fefilova, A.S., Zatsepin, T.S., Bogorad, R.L., Baranov, P.V., Langer, R.*, et al.* (2020). In Vivo RNAi-Mediated eIF3m Knockdown Affects Ribosome Biogenesis and Transcription but Has Limited Impact on mRNA-Specific Translation. Mol Ther Nucleic Acids *19*, 252-266.
Sodani, K., Patel, A., Kathawala, R.J., and Chen, Z.S. (2012). Multidrug resistance associated proteins in multidrug resistance. Chin J Cancer *31*, 58-72.
Sonenberg, N., and Hinnebusch, A.G. (2009). Regulation of Translation Initiation in Eukaryotes: Mechanisms and Biological Targets. Cell *136*, 731-745.

Spilka, R., Ernst, C., Mehta, A.K., and Haybaeck, J. (2013). Eukaryotic translation initiation factors in cancer development and progression. Cancer Lett *340*, 9-21.
Sriram, A., Bohlen, J., and Teleman, A.A. (2018). Translation acrobatics: how cancer cells exploit alternate modes of translational initiation. EMBO Rep *19*.
Stokoe, D., Macdonald, S.G., Cadwallader, K., Symons, M., and Hancock, J.F. (1994). Activation of Raf as a result of recruitment to the plasma membrane. Science *264*, 1463-1467.
Stolovich, M., Tang, H., Hornstein, E., Levy, G., Cohen, R., Bae, S.S., Birnbaum, M.J., and Meyuhas, O. (2002). Transduction of growth or mitogenic signals into translational activation of TOP mRNAs is fully reliant on the phosphatidylinositol 3-kinase-mediated pathway but requires neither S6K1 nor rpS6 phosphorylation. Mol Cell Biol *22*, 8101-8113.
Topisirovic, I., Ruiz-Gutierrez, M., and Borden, K.L. (2004). Phosphorylation of the eukaryotic translation initiation factor eIF4E contributes to its transformation and mRNA transport activities. Cancer Res *64*, 8639-8642.
Truitt, M.L., and Ruggero, D. (2016). New frontiers in translational control of the cancer genome. Nat Rev Cancer *16*, 288-304.
Tweedie, S., Braschi, B., Gray, K., Jones, T.E.M., Seal, R.L., Yates, B., and Bruford, E.A. (2021). Genenames.org: the HGNC and VGNC resources in 2021. Nucleic Acids Res *49*, D939-D946.
Valášek, L.S. (2012). 'Ribozoomin' – Translation Initiation from the Perspective of the Ribosome-bound Eukaryotic Initiation Factors (eIFs). Curr Protein Pept Sci *13*, 305-330.
Valasek, L.S., Zeman, J., Wagner, S., Beznoskova, P., Pavlikova, Z., Mohammad, M.P., Hronova, V., Herrmannova, A., Hashem, Y., and Gunisova, S. (2017). Embraced by eIF3: structural and functional insights into the roles of eIF3 across the translation cycle. Nucleic Acids Res *45*, 10948-10968.
Vattem, K.M., and Wek, R.C. (2004). Reinitiation involving upstream ORFs regulates ATF4 mRNA translation in mammalian cells. Proc Natl Acad Sci U S A *101*, 11269-11274.
Volta, V., Perez-Baos, S., de la Parra, C., Katsara, O., Ernlund, A., Dornbaum, S., and Schneider, R.J. (2021). A DAP5/eIF3d alternate mRNA translation mechanism promotes differentiation and immune suppression by human regulatory T cells. Nat Commun *12*, 6979.
Wagner, S., Herrmannová, A., Hronová, V., Gunišová, S., Sen, N.D., Hannan, R.D., Hinnebusch, A.G., Shirokikh, N.E., Preiss, T., and Valášek, L.S. (2020). Selective Translation Complex Profiling Reveals Staged Initiation and Co-translational Assembly of Initiation Factor Complexes. Mol Cell *79*, 546-560 e547.
Wagner, S., Herrmannova, A., Malik, R., Peclinovska, L., and Valasek, L.S. (2014). Functional and Biochemical Characterization of Human Eukaryotic Translation Initiation Factor 3 in Living Cells. Mol Cell Biol *34*, 3041-3052.
Wagner, S., Herrmannova, A., Sikrova, D., and Valasek, L.S. (2016). Human eIF3b and eIF3a serve as the nucleation core for the assembly of eIF3 into two interconnected modules: the yeast-like core and the octamer. Nucleic Acids Res *44*, 10772-10788.
Waskiewicz, A.J., Flynn, A., Proud, C.G., and Cooper, J.A. (1997). Mitogen-activated protein kinases activate the serine/threonine kinases Mnk1 and Mnk2. EMBO J *16*, 1909-1920.

Wolf, D.A., Lin, Y., Duan, H., and Cheng, Y. (2020). eIF-Three to Tango: emerging functions of translation initiation factor eIF3 in protein synthesis and disease. J Mol Cell Biol *12*, 403-409.
Xia, Y., Shen, S., and Verma, I.M. (2014). NF-kappaB, an active player in human cancers. Cancer Immunol Res *2*, 823-830.
Zhang, L., Pan, X., and Hershey, J.W. (2007). Individual overexpression of five subunits of human translation initiation factor eIF3 promotes malignant transformation of immortal fibroblast cells. J Biol Chem *282*, 5790-5800.
Zhang, W., and Liu, H.T. (2002). MAPK signal pathways in the regulation of cell proliferation in mammalian cells. Cell Res *12*, 9-18.
Zhang, Y., and Wang, X. (2020). Targeting the Wnt/beta-catenin signaling pathway in cancer. J Hematol Oncol *13*, 165.

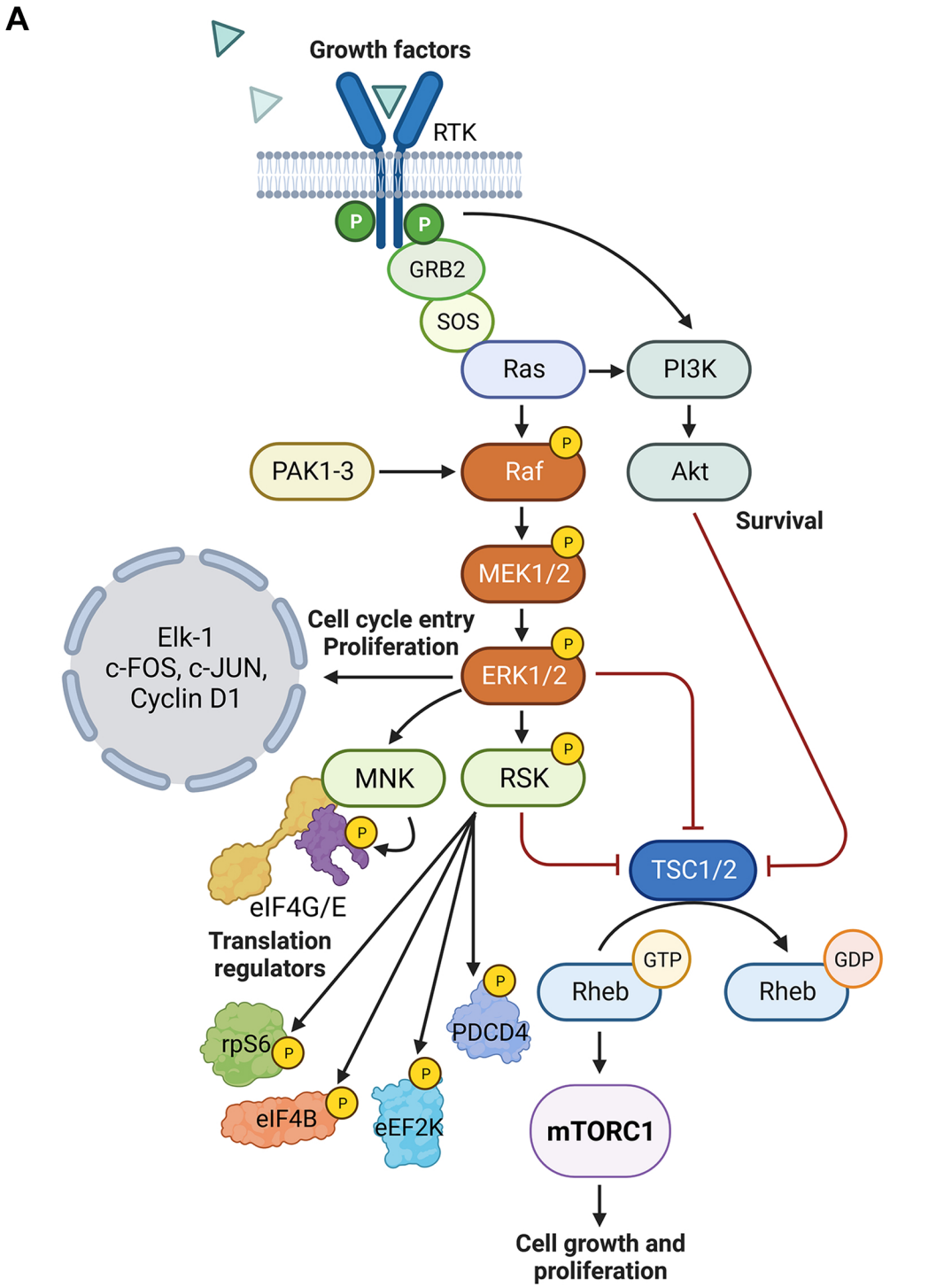
A
Growth factors
RTK
P
P
GRB2
SOS
Ras
PI3K
PAK1-3
Raf
Akt
Survival
MEK1/2
Elk-1
c-FOS, c-JUN,
Cyclin D1
Cell cycle entry
Proliferation
ERK1/2
MNK
RSK
eIF4G/E
Translation
regulators
TSC1/2
GTP
GDP
Rheb
Rheb
rpS6
PDCD4
eIF4B
eEF2K
mTORC1
Cell growth and
proliferation

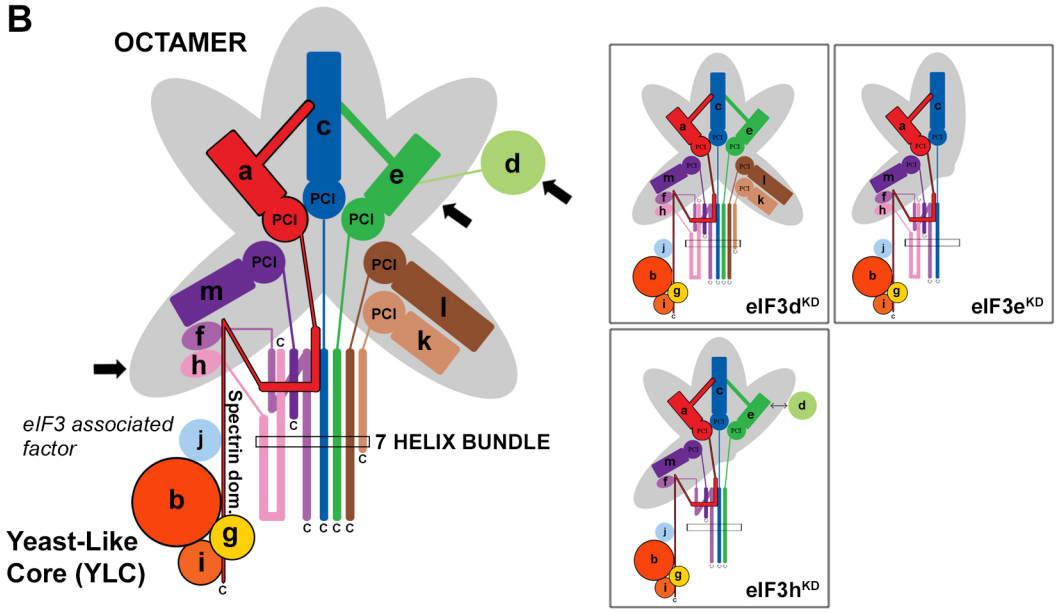
B
OCTAMER
PCI
eIF3 associated
factor
Spectrin dom.
7 HELIX BUNDLE
Yeast-Like
Core (YLC)
eIF3d^KD
eIF3e^KD
eIF3h^KD

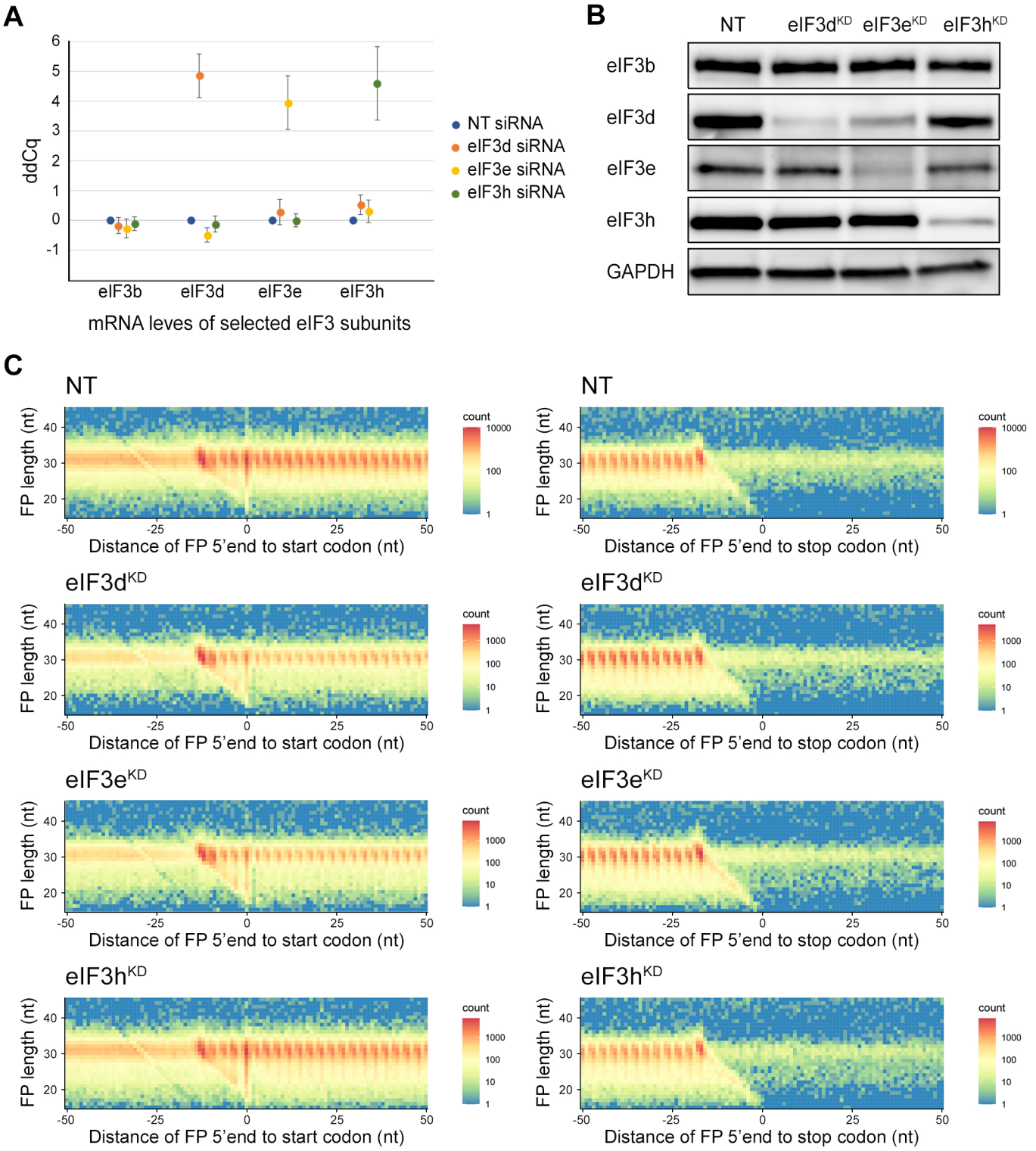
A
ddCq
6
5
4
3
2
1
0
-1
eIF3b
eIF3d
eIF3e
eIF3h
mRNA leves of selected eIF3 subunits
NT siRNA
eIF3d siRNA
eIF3e siRNA
eIF3h siRNA
B
NT
eIF3d^KD
eIF3e^KD
eIF3h^KD
eIF3b
eIF3d
eIF3e
eIF3h
GAPDH
C
NT
eIF3d^KD
eIF3e^KD
eIF3h^KD
FP length (nt)
Distance of FP 5'end to start codon (nt)
Distance of FP 5'end to stop codon (nt)
count
10000
1000
100
10
1
-50
-25
0
25
50
20
30
40

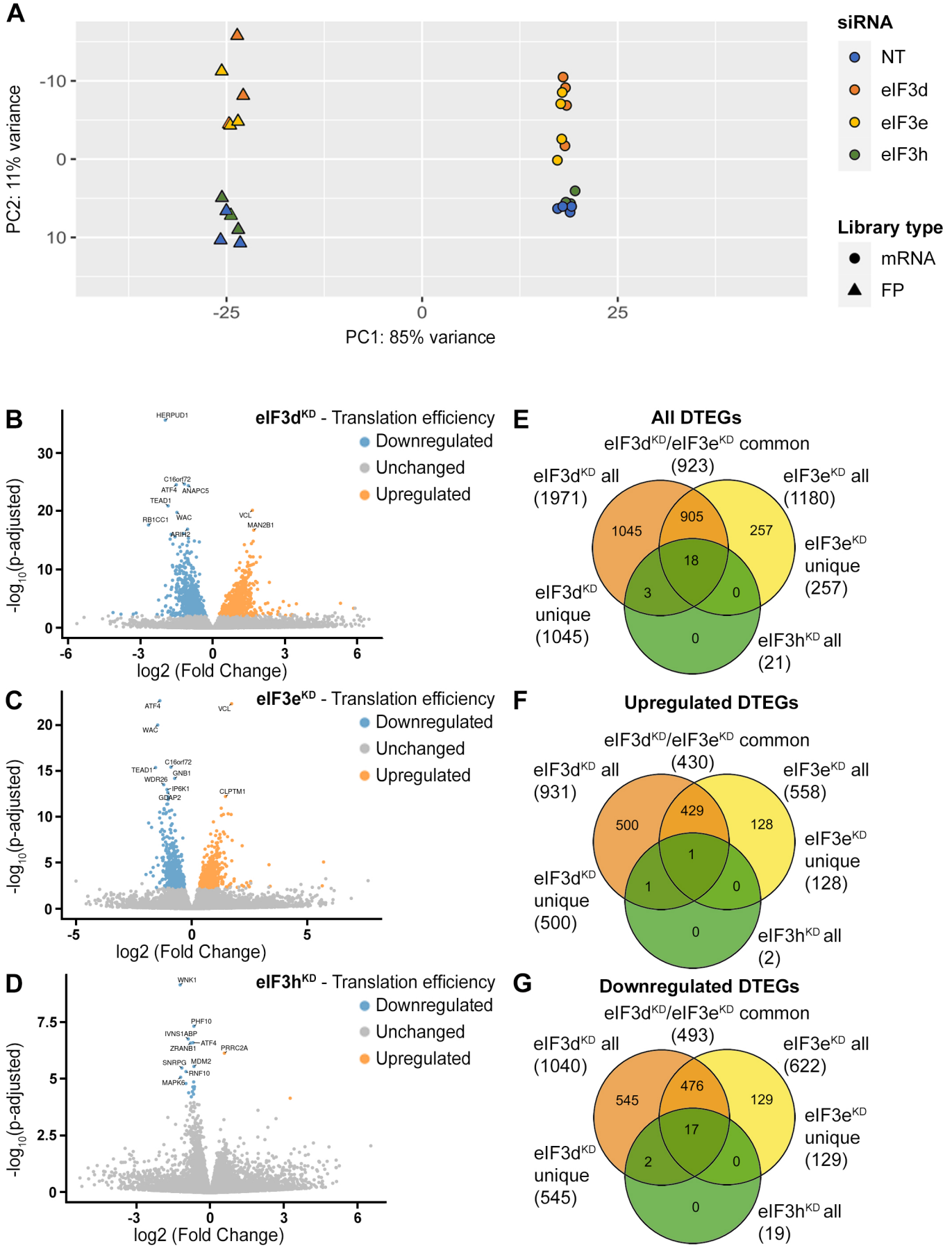
A
PC2: 11% variance
PC1: 85% variance
siRNA
NT
eIF3d
eIF3e
eIF3h
Library type
mRNA
FP
B
eIF3d^KD - Translation efficiency
Downregulated
Unchanged
Upregulated
-log10(p-adjusted)
log2 (Fold Change)
HERPUD1
C16orf72
ATF4
ANAPC5
TEAD1
RB1CC1
WAC
ARIH2
VCL
MAN2B1
C
eIF3e^KD - Translation efficiency
ATF4
VCL
WAC
C16orf72
TEAD1
GNB1
WDR26
IP6K1
GDAP2
CLPTM1
D
eIF3h^KD - Translation efficiency
WNK1
PHF10
IVNS1ABP
ATF4
ZRANB1
PRRC2A
SNRPG
MDM2
RNF10
MAPK6
E
All DTEGs
eIF3d^KD/eIF3e^KD common (923)
eIF3d^KD all (1971)
eIF3e^KD all (1180)
eIF3e^KD unique (257)
eIF3d^KD unique (1045)
eIF3h^KD all (21)
1045
905
257
18
3
0
0
F
Upregulated DTEGs
eIF3d^KD/eIF3e^KD common (430)
eIF3d^KD all (931)
eIF3e^KD all (558)
eIF3e^KD unique (128)
eIF3d^KD unique (500)
eIF3h^KD all (2)
500
429
128
1
1
0
0
G
Downregulated DTEGs
eIF3d^KD/eIF3e^KD common (493)
eIF3d^KD all (1040)
eIF3e^KD all (622)
eIF3e^KD unique (129)
eIF3d^KD unique (545)
eIF3h^KD all (19)
545
476
129
17
2
0
0

A KEGG enrichment analysis

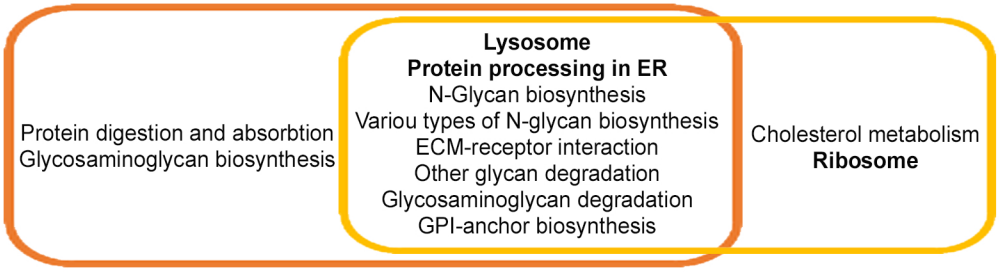

B

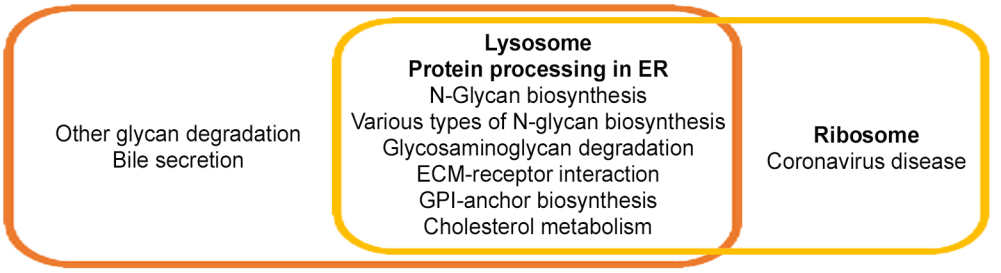

C eIF3e^KD "unique upregulated" DTEGs

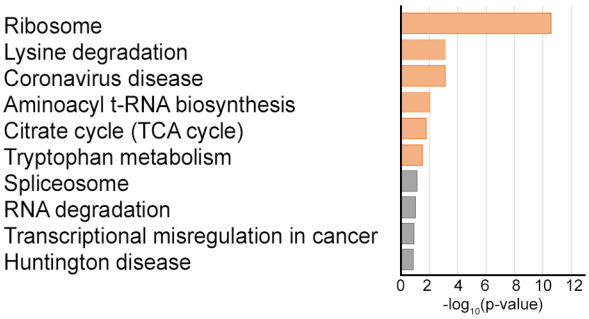

D

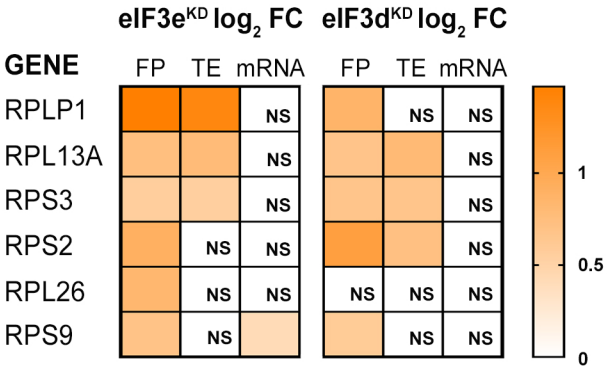

E

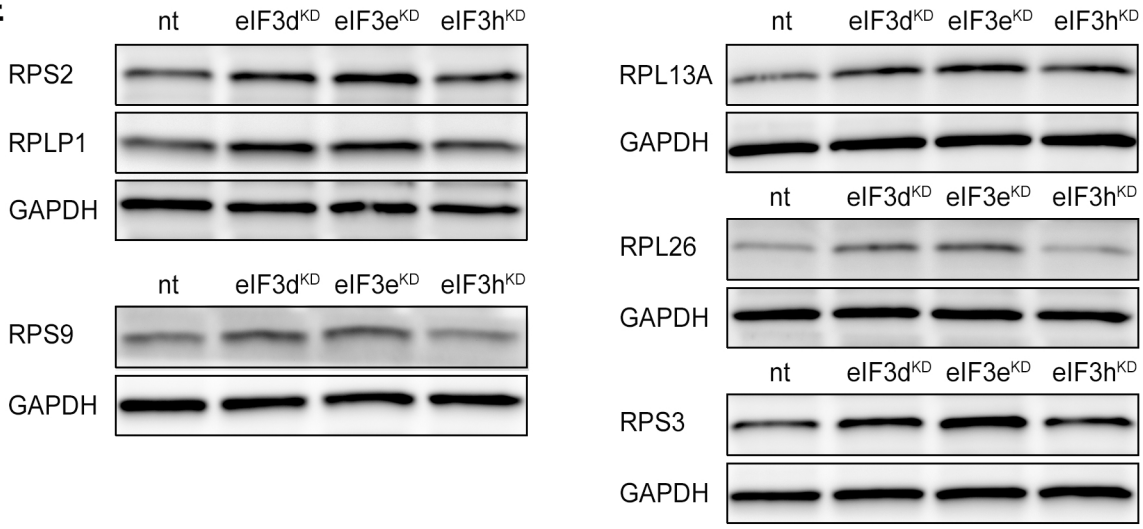

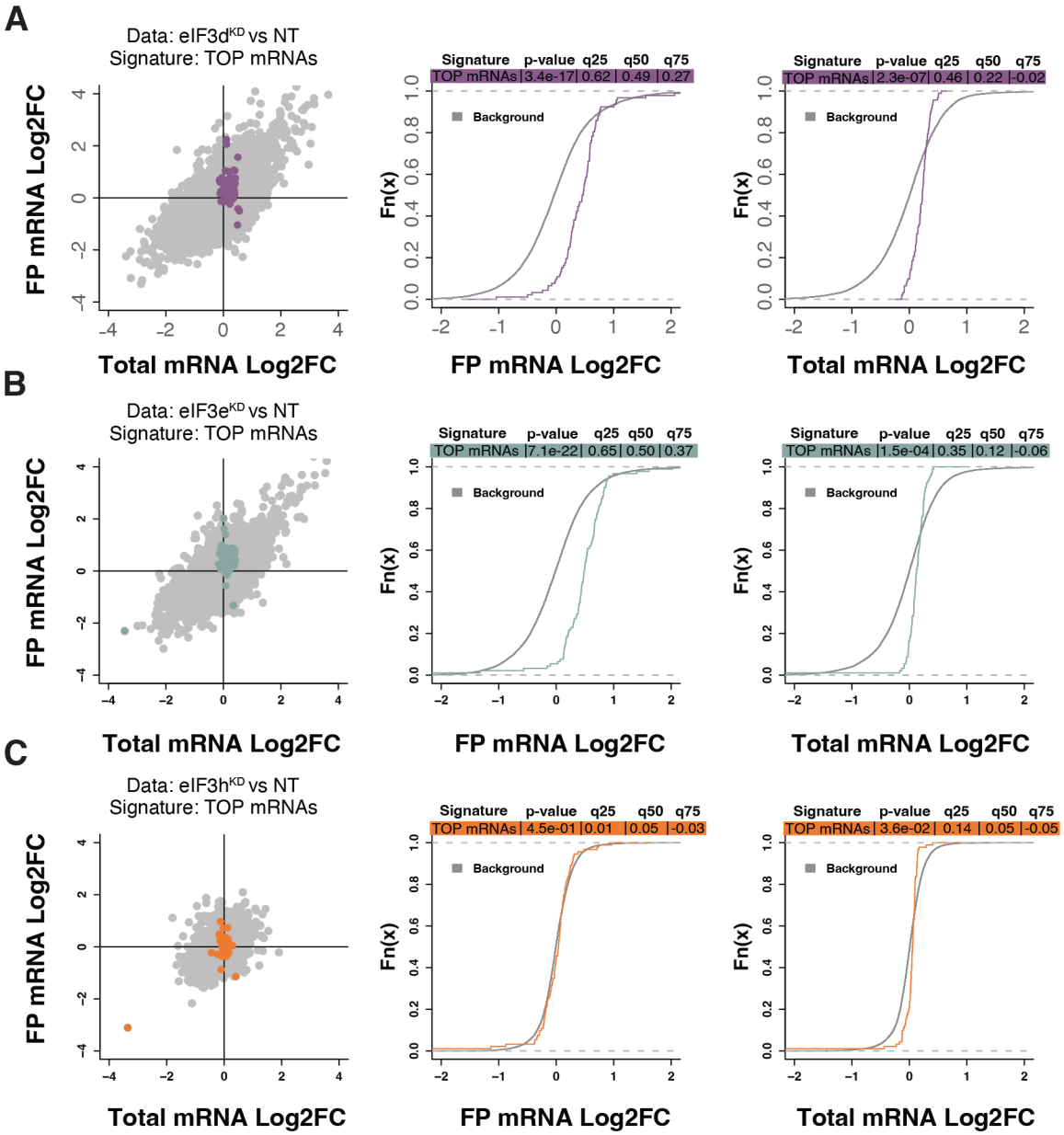
A
Data: eIF3d^KD vs NT
Signature: TOP mRNAs
FP mRNA Log2FC
Total mRNA Log2FC
Signature p-value q25 q50 q75
TOP mRNAs 3.4e-17 0.62 0.49 0.27
Background
Fn(x)
FP mRNA Log2FC
Signature p-value q25 q50 q75
TOP mRNAs 2.3e-07 0.46 0.22 -0.02
Background
Fn(x)
Total mRNA Log2FC
B
Data: eIF3e^KD vs NT
Signature: TOP mRNAs
FP mRNA Log2FC
Total mRNA Log2FC
Signature p-value q25 q50 q75
TOP mRNAs 7.1e-22 0.65 0.50 0.37
Background
Fn(x)
FP mRNA Log2FC
Signature p-value q25 q50 q75
TOP mRNAs 1.5e-04 0.35 0.12 -0.06
Background
Fn(x)
Total mRNA Log2FC
C
Data: eIF3h^KD vs NT
Signature: TOP mRNAs
FP mRNA Log2FC
Total mRNA Log2FC
Signature p-value q25 q50 q75
TOP mRNAs 4.5e-01 0.01 0.05 -0.03
Background
Fn(x)
FP mRNA Log2FC
Signature p-value q25 q50 q75
TOP mRNAs 3.6e-02 0.14 0.05 -0.05
Background
Fn(x)
Total mRNA Log2FC

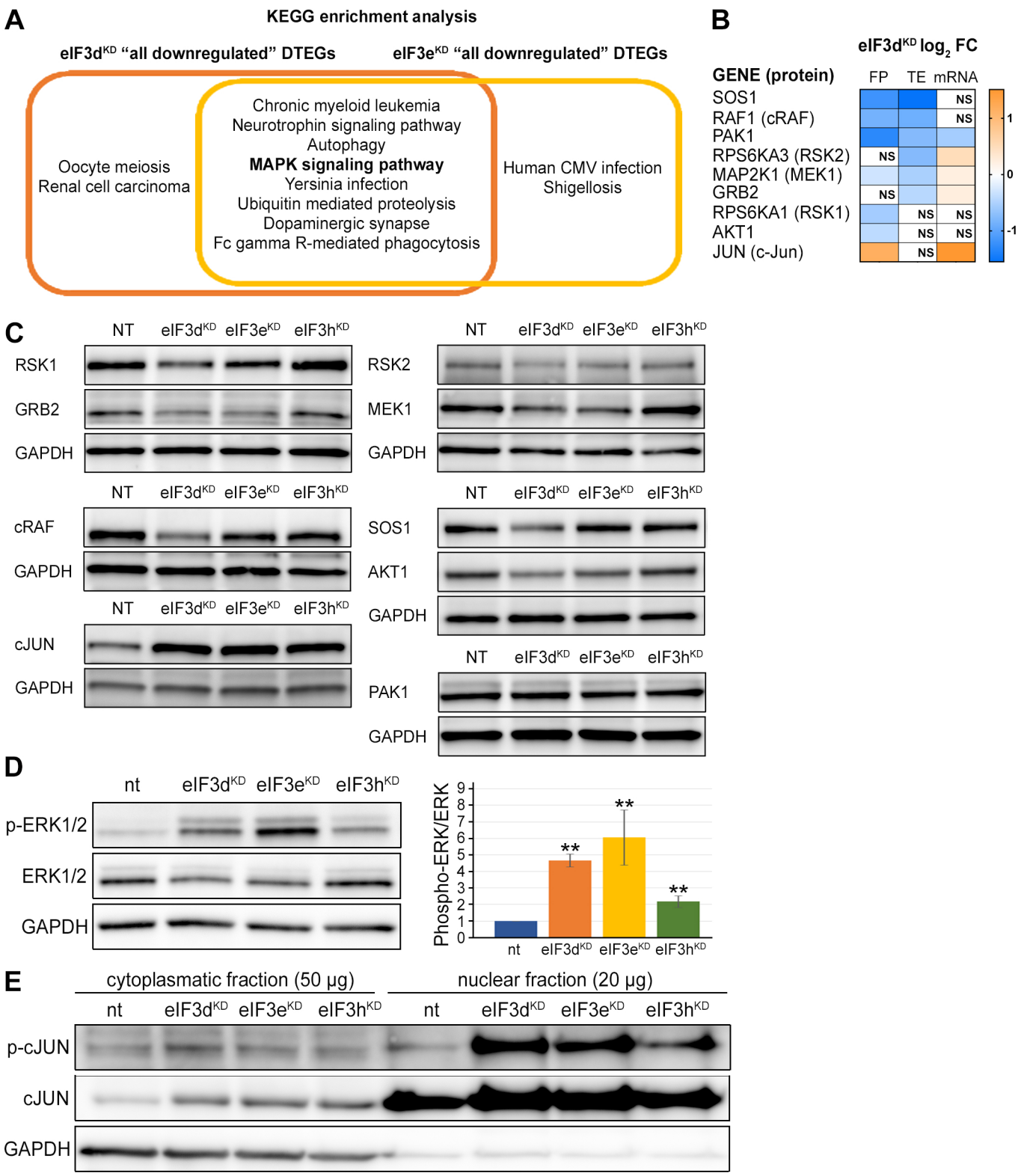
A
KEGG enrichment analysis
eIF3d^KD "all downregulated" DTEGs
eIF3e^KD "all downregulated" DTEGs
Oocyte meiosis
Renal cell carcinoma
Chronic myeloid leukemia
Neurotrophin signaling pathway
Autophagy
MAPK signaling pathway
Yersinia infection
Ubiquitin mediated proteolysis
Dopaminergic synapse
Fc gamma R-mediated phagocytosis
Human CMV infection
Shigellosis
B
eIF3d^KD log2 FC
GENE (protein)
FP
TE
mRNA
SOS1
RAF1 (cRAF)
PAK1
RPS6KA3 (RSK2)
MAP2K1 (MEK1)
GRB2
RPS6KA1 (RSK1)
AKT1
JUN (c-Jun)
NS
1
0
-1
C
NT
eIF3d^KD
eIF3e^KD
eIF3h^KD
RSK1
GRB2
GAPDH
RSK2
MEK1
cRAF
SOS1
AKT1
cJUN
PAK1
D
nt
p-ERK1/2
ERK1/2
Phospho-ERK/ERK
**
E
cytoplasmatic fraction (50 µg)
nuclear fraction (20 µg)
p-cJUN
cJUN

A **eIF3h^{KD} "all downregulated" DTEGs**

KEGG enrichment analysis

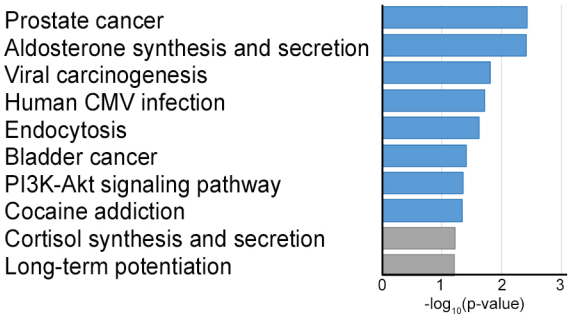

B **eIF3h^{KD} all downregulated DTEGs**

GO biological process enrichment analysis

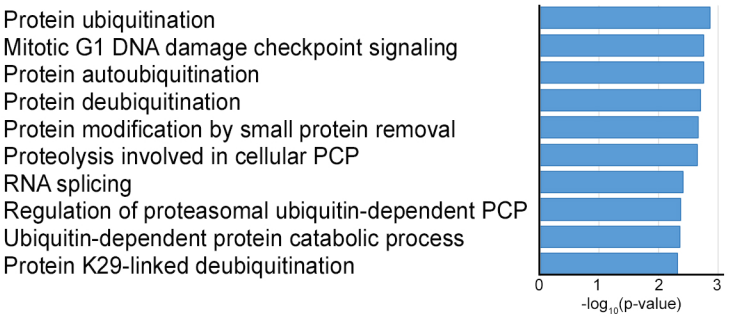

C

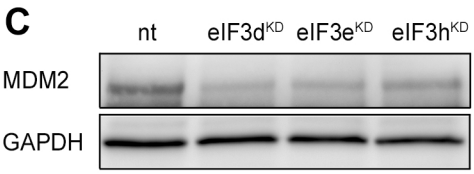

D

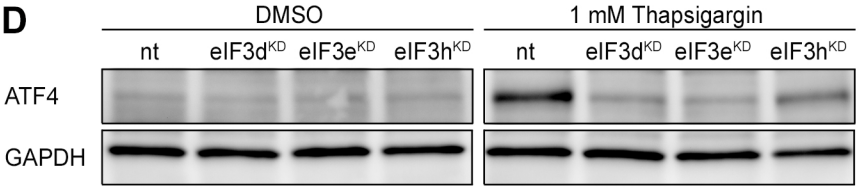

E

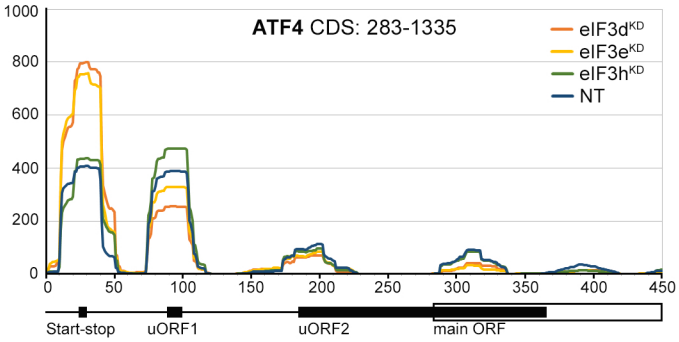

F

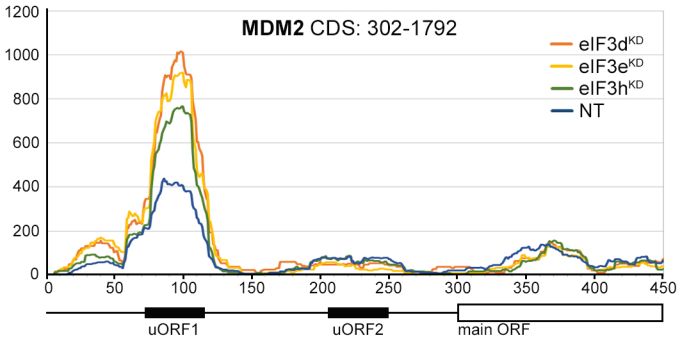

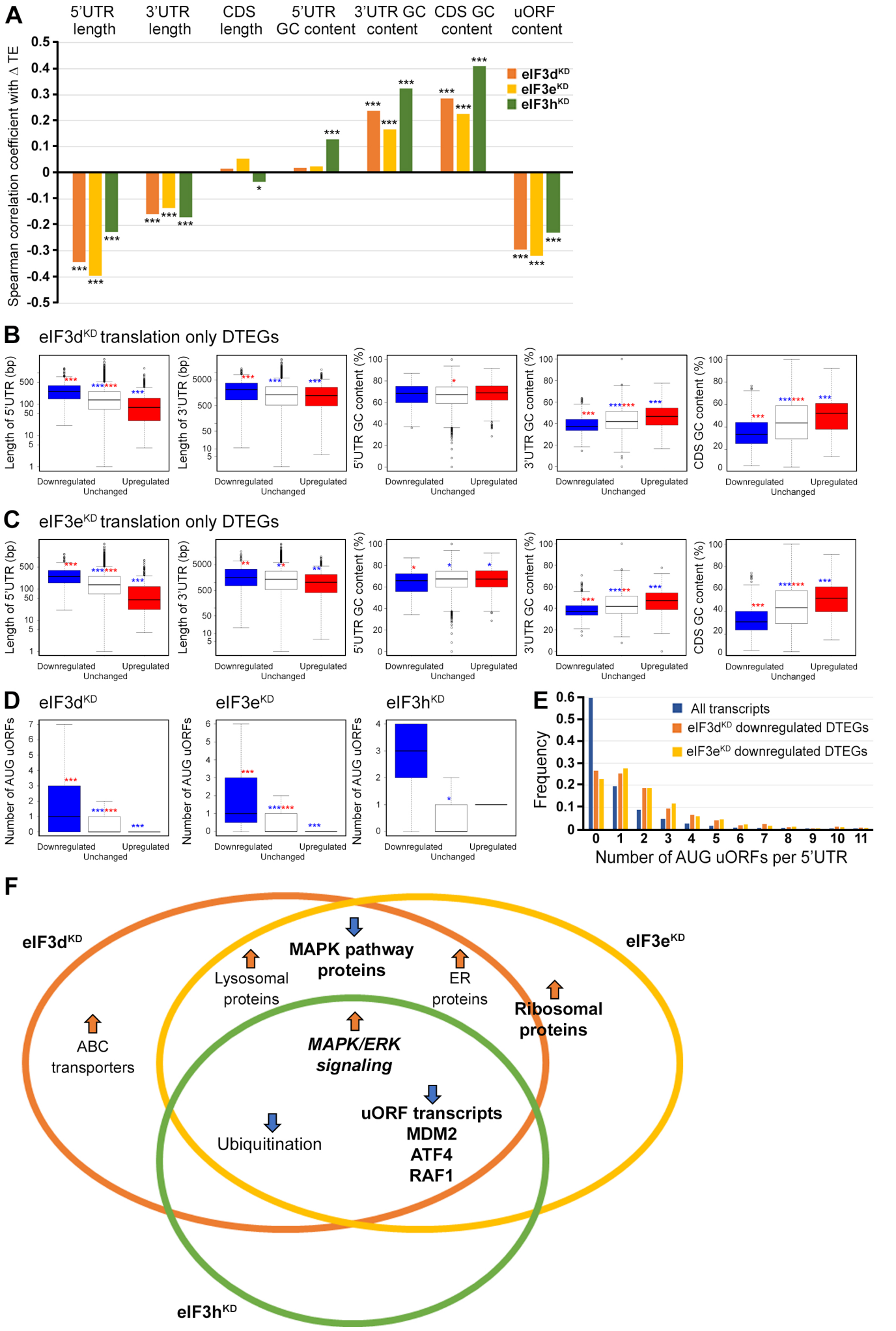
A
5'UTR length
3'UTR length
CDS length
5'UTR GC content
3'UTR GC content
CDS GC content
uORF content
Spearman correlation coefficient with Δ TE
eIF3d^KD
eIF3e^KD
eIF3h^KD
B
eIF3d^KD translation only DTEGs
Length of 5'UTR (bp)
Length of 3'UTR (bp)
5'UTR GC content (%)
3'UTR GC content (%)
CDS GC content (%)
Downregulated
Unchanged
Upregulated
C
eIF3e^KD translation only DTEGs
D
eIF3d^KD
eIF3e^KD
eIF3h^KD
Number of AUG uORFs
E
All transcripts
eIF3d^KD downregulated DTEGs
eIF3e^KD downregulated DTEGs
Frequency
Number of AUG uORFs per 5'UTR
F
eIF3d^KD
eIF3e^KD
eIF3h^KD
MAPK pathway proteins
Lysosomal proteins
ER proteins
Ribosomal proteins
ABC transporters
MAPK/ERK signaling
Ubiquitination
uORF transcripts
MDM2
ATF4
RAF1

Supplementary Information

Perturbations in eIF3 subunit stoichiometry alter expression of ribosomal proteins and key components of the MAPK signaling pathway.

Anna Herrmannová[1#*], Jan Jelínek[2#], Klára Pospíšilová[1], Farkas Kerényi[1], Tomáš Vomastek[3], Kathleen Watt[4], Jan Brábek[5], Mahabub Pasha Mohammad[1], Susan Wagner[1], Ivan Topisirovic[6], and Leoš Shivaya Valášek[1*]

[1]Laboratory of Regulation of Gene Expression, Institute of Microbiology of the Czech Academy of Sciences, Prague, Videnska 1083, 142 20, the Czech Republic
[2]Laboratory of Bioinformatics, Institute of Microbiology of the Czech Academy of Sciences, Prague, Videnska 1083, 142 20, the Czech Republic
[3]Laboratory of Cell Signaling, Institute of Microbiology of the Czech Academy of Sciences, Prague, Videnska 1083, 142 20, the Czech Republic
[4] Science for Life Laboratory, Department of Oncology-Pathology, Karolinska Institutet, Solna, Sweden
[5]Laboratory of Cancer Cell Invasion, Faculty of Science, Charles University, Prague,
Vinicna 7, 128 43, Czech Republic
[6]Lady Davis Institute, Gerald Bronfman Department of Oncology, Department of Biochemistry, Division of Experimental Medicine, McGill University, Montréal, H3T 1E2, QC Canada

[#] These authors contributed equally to this work.

* To whom the correspondence should be addressed: herrmannova@seznam.cz
valasekl@biomed.cas.cz
Tel: +420 241 062 288
Fax: +420 241 062 665

Supplementary Figures

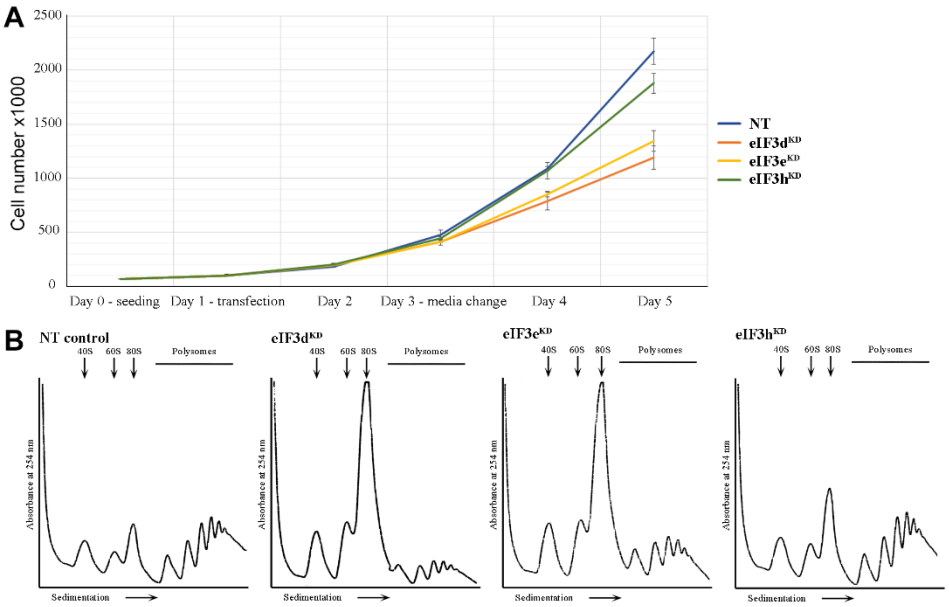

Supplementary Figure 1. **Hela cells downregulated for eIF3d, eIF3e and eIF3h display slower growth and impaired translation. (A)** Growth curve of Hela cells transfected with siRNA targeting eIF3d, eIF3e, eIF3h or non-targeting (NT) siRNA as a control. Cells were grown in 6 well plates in duplicates and counted by Corning cell counter. **(B)** Standard polysome profiles illustrate that cells were not overgrown at the time of harvest and occurred in a state of active translation (NT) with the expected specific reduction in polysomes in all three knock-downs, as reported previously (Wagner et al., 2016). One example profile for each knock-down is shown.

A Spearman correlation between replicates

nt_FP	rep_1	rep_2
rep_1		
rep_2	0.989	
rep_3	0.985	0.986

d_FP	rep_1	rep_2
rep_1		
rep_2	0.981	
rep_3	0.976	0.984

e_FP	rep_1	rep_2
rep_1		
rep_2	0.984	
rep_3	0.982	0.986

h_FP	rep_1	rep_2
rep_1		
rep_2	0.986	
rep_3	0.985	0.989

nt_mRNA	rep_1	rep_2	rep_3
rep_1			
rep_2	0.994		
rep_3	0.988	0.990	
rep_4	0.994	0.994	0.990

d_mRNA	rep_1	rep_2	rep_3
rep_1			
rep_2	0.984		
rep_3	0.992	0.989	
rep_4	0.992	0.986	0.993

e_mRNA	rep_1	rep_2	rep_3
rep_1			
rep_2	0.990		
rep_3	0.993	0.993	
rep_4	0.994	0.991	0.994

h_mRNA	rep_1	rep_2	rep_3
rep_1			
rep_2	0.994		
rep_3	0.992	0.993	
rep_4	0.989	0.988	0.988

B Readlength distribution of FP

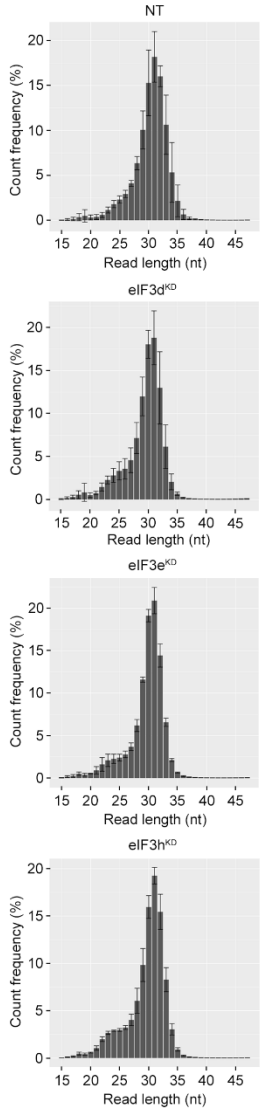

C 3nt periodicity in CDS

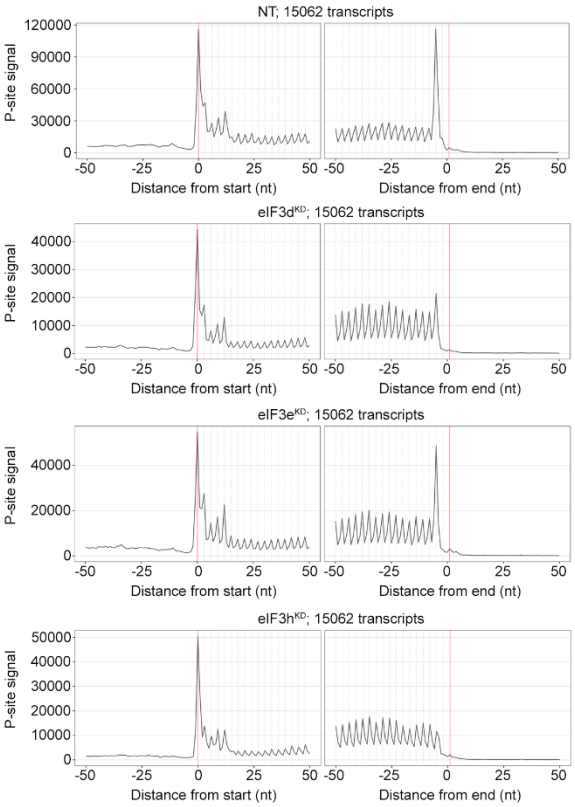

D Read distribution (absolute counts)

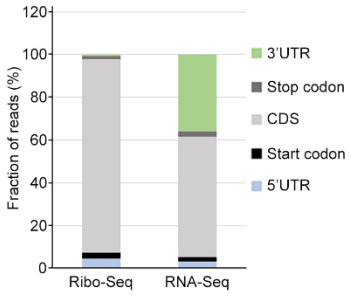

E Read distribution (length normalised)

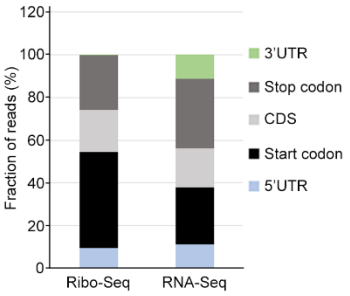

Supplementary Figure 2. **Quality control of Ribo-Seq libraries from all eIF3 knock-downs and the NT control. (A)** Spearman correlation coefficients of the footprint or mRNA count per gene among all replicates. **(B)** Read length distribution of footprints in Ribo-Seq libraries from all eIF3 knock-downs and the NT control. Bar charts show average values for each fragment length (after alignment to genome); all Ribo-Seq libraries were done in triplicates. **(C)** Meta-profiles showing the periodicity of ribosomes along the transcripts at the genome-wide scale. The metaprofiles are based on the P-site identification obtained by using riboWaltz (Lauria et al., 2018). **(D)** Fraction of reads in different transcript features **(E)** Same as in (D) but numbers of reads in each feature were normalized for average feature length.

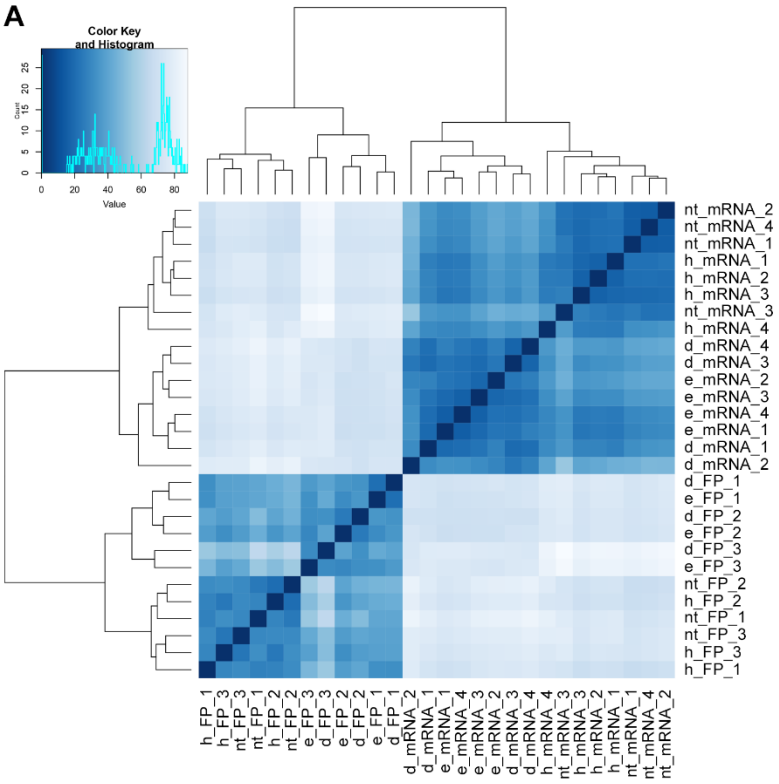
A
Color Key
and Histogram
Count
Value
nt_mRNA_2
nt_mRNA_4
nt_mRNA_1
h_mRNA_1
h_mRNA_2
h_mRNA_3
nt_mRNA_3
h_mRNA_4
d_mRNA_4
d_mRNA_3
e_mRNA_2
e_mRNA_3
e_mRNA_4
e_mRNA_1
d_mRNA_1
d_mRNA_2
d_FP_1
e_FP_1
d_FP_2
e_FP_2
d_FP_3
e_FP_3
nt_FP_2
h_FP_2
nt_FP_1
nt_FP_3
h_FP_3
h_FP_1

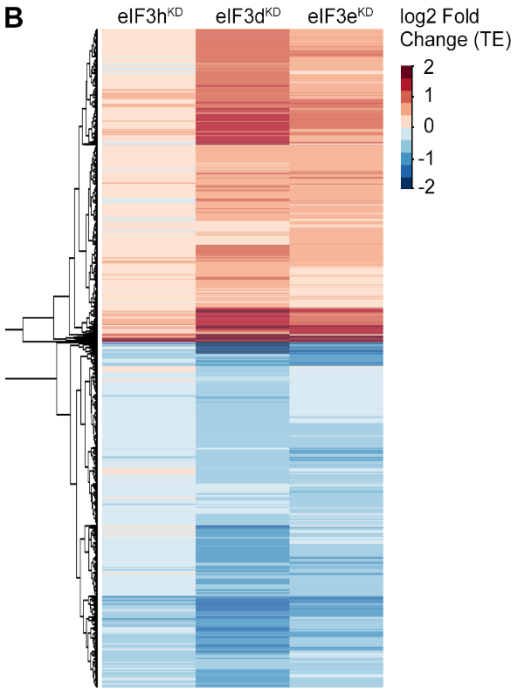
B
eIF3h^KD
eIF3d^KD
eIF3e^KD
log2 Fold
Change (TE)
2
1
0
-1
-2

Supplementary Figure 3. **Clustering of Ribo-Seq and RNA-Seq libraries and Differential Translation Efficiency Genes (DTEGs). (A)** Heatmap and dendrogram resulting from hierarchical clustering analysis of Ribo-Seq libraries and RNA-Seq libraries. Analysis was performed on gene counts by DESeq2 (Love et al., 2014) and biomaRt (Durinck et al., 2009). **(B)** Heatmap and dendrogram resulting from hierarchical clustering analysis of significant TE changes observed in eIF3d^{KD}, eIF3e^{KD} and eIF3h^{KD} cells.

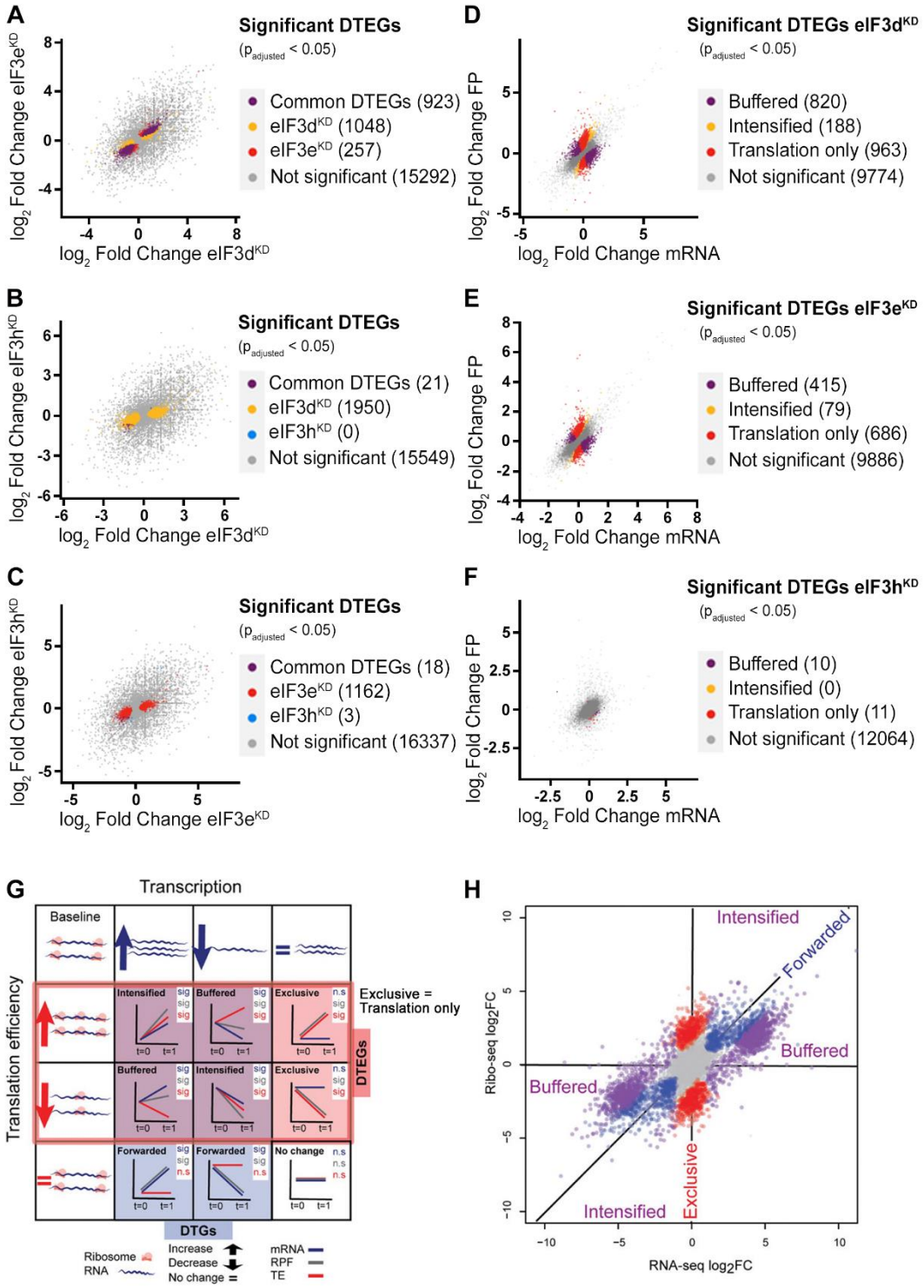
A
Significant DTEGs
($p_{adjusted}$ < 0.05)
Common DTEGs (923)
eIF3d^{KD} (1048)
eIF3e^{KD} (257)
Not significant (15292)
log$_2$ Fold Change eIF3e^{KD}
log$_2$ Fold Change eIF3d^{KD}
B
Significant DTEGs
($p_{adjusted}$ < 0.05)
Common DTEGs (21)
eIF3d^{KD} (1950)
eIF3h^{KD} (0)
Not significant (15549)
log$_2$ Fold Change eIF3h^{KD}
log$_2$ Fold Change eIF3d^{KD}
C
Significant DTEGs
($p_{adjusted}$ < 0.05)
Common DTEGs (18)
eIF3e^{KD} (1162)
eIF3h^{KD} (3)
Not significant (16337)
log$_2$ Fold Change eIF3h^{KD}
log$_2$ Fold Change eIF3e^{KD}
D
Significant DTEGs eIF3d^{KD}
($p_{adjusted}$ < 0.05)
Buffered (820)
Intensified (188)
Translation only (963)
Not significant (9774)
log$_2$ Fold Change FP
log$_2$ Fold Change mRNA
E
Significant DTEGs eIF3e^{KD}
($p_{adjusted}$ < 0.05)
Buffered (415)
Intensified (79)
Translation only (686)
Not significant (9886)
log$_2$ Fold Change FP
log$_2$ Fold Change mRNA
F
Significant DTEGs eIF3h^{KD}
($p_{adjusted}$ < 0.05)
Buffered (10)
Intensified (0)
Translation only (11)
Not significant (12064)
log$_2$ Fold Change FP
log$_2$ Fold Change mRNA
G
Transcription
Baseline
Translation efficiency
Intensified
Buffered
Exclusive
Forwarded
No change
Exclusive = Translation only
DTEGs
DTGs
Ribosome
RNA
Increase
Decrease
No change
mRNA
RPF
TE
H
Intensified
Forwarded
Buffered
Buffered
Exclusive
Intensified
Ribo-seq log2FC
RNA-seq log2FC

Supplementary Figure 4. **DTEGs identified in all knock-downs largely overlap. (A-C)** Scatter plots of genes with significant TE changes and their overlap in individual knock-downs. **(A)** eIF3d^{KD} vs. eIF3e^{KD} **(B)** eIF3d^{KD} vs. eIF3h^{KD} **(C)** eIF3e^{KD} vs. eIF3h^{KD}. **(D-F)** Scatter plots showing classification of significant DTEGs into different groups based on fold changes of FP and mRNA. Buffered DTEGs (purple) display a significant change in TE that counteracts the change in mRNA, hence buffering the effect of transcription. Translation only DTEGs (red) have a significant change in FP while maintaining the same mRNA levels, which results in a significant change in TE. Translationally intensified DTEGs (yellow) have a significant change in TE that occurs in the same direction as the effect of transcription (i.e., a gene exhibiting an increase in transcription also exhibits increase in TE that altogether boost protein production). **(D)** eIF3d^{KD}, **(E)** eIF3e^{KD}, **(F)** eIF3h^{KD}. (**G** - **H**) Classification of genes based on fold changes of FP (RFP), mRNA, and TE (adopted from (Chothani et al., 2019) with permission). (**G**) A gene could be either/both DTG (Differentially Transcribed Gene) and/or DTEG (Differential Translation Efficiency Gene), and based on the direction of change would fall into one of the eight gene-regulatory possibilities (sig: significant, n.s.: not significant). Translationally forwarded genes are DTGs that have a significant change in mRNA and FP at the same rate, with no significant change in TE. Conversely, translationally exclusive / translation only genes are DTEGs that have a significant change in FP, with no change in mRNA leading to a significant change in TE. Several genes are both DTGs and DTEGs, and their regulatory class is determined based on a combination of the relative direction of change between transcription and translation efficiency. Specifically, translationally buffered genes have a significant change in TE that counteracts the change in mRNA; hence, buffering the effect of transcription. Translationally intensified genes have a significant change in TE that acts with the effect of transcription. In all cases, the change in mRNA can be either positive or negative, and where buffering or intensifying takes place, the direction of change is taken into account. For example, a gene that exhibits an increase in transcription and an increase in translation efficiency is classified as intensified, while a gene that exhibits an increase in transcription but a decrease in translational efficiency is classified as buffered. (**H**) Simulated data showing fold changes for each gene in RNA-seq and Ribo-seq data. Translationally forwarded genes (in blue), exclusive (translation only) genes (in red), buffered genes (in purple), and intensified genes (in purple) are highlighted.

A

		eIF3dKD all upregulated			eIF3eKD all upregulated			eIF3dKD/eIF3eKD common			eIF3dKD unique upregulated			eIF3dKD translation only upregulated			eIF3eKD translation only upregulated		
KEGG term	# of genes in pathway	rank	p-value	# of genes	rank	p-value	# of genes	rank	p-value	# of genes	rank	p-value	# of genes	rank	p-value	# of genes	rank	p-value	# of genes
Lysosome	132	1	1.56E-34	* 51	1	8.29E-22	* 32	1	2.67E-25	* 32	1	4.59E-10	* 19	1	1.48E-26	* 36	1	3.99E-18	* 25
Protein processing in ER	171	2	1.13E-24	* 48	2	6.21E-16	* 30	2	4.64E-19	* 30	2	3.05E-07	* 18	2	5.94E-18	* 32	2	5.33E-17	* 27
N-Glycan biosynthesis	50	3	1.44E-20	* 25	3	2.11E-13	* 16	3	3.71E-15	* 16	5	3.57E-06	* 9	3	2.83E-12	* 15	3	9.82E-12	* 13
Various types of N-glycan biosynthesis	39	4	3.67E-13	* 17	5	5.75E-09	* 11	4	3.71E-10	* 11	11	3.84E-04	* 6	4	1.8E-11	* 13	4	1.5E-10	* 11
ECM-receptor interaction	88	5	8.19E-12	* 23	7	9.18E-07	* 13	6	4.61E-08	* 13	9	6.87E-05	* 10	6	7.81E-07	* 13	6	1.69E-08	* 13
Other glycan degradation	18	6	1.39E-09	* 10	10	1.03E-04	* 5	10	2.98E-05	* 5	8	6.26E-05	* 5	8	5.77E-06	* 6	17	4.93E-03	3
Protein digestion and absorption	103	7	1.56E-09	* 22	12	5.92E-04	* 10	11	7.27E-05	* 10	7	1.02E-05	* 12	12	2.52E-05	* 12	15	4.23E-03	* 7
Glycosaminoglycan degradation	19	8	2.81E-09	* 10	8	8.95E-06	* 6	7	1.99E-06	* 6	13	1.11E-03	* 4	5	1.75E-08	* 8	8	2.65E-05	* 5
GPI-anchor biosynthesis	26	9	8.33E-09	* 11	6	1.90E-08	* 9	5	4.59E-08	* 8	32	0.026359	3	7	4.67E-06	* 7	7	9.14E-06	* 6
Glycosaminoglycan biosynthesis	20	10	6.43E-07	* 9	40	NS	3	34	0.026581	3	6	5.92E-06	* 6	19	5.77E-04	* 4	57	NS	1
ABC transporters	45	11	6.53E-07	* 12	49	NS	3	43	NS	3	3	1.41E-06	* 9	13	2.66E-05	* 8	52	NS	2
Phagosome	152	13	2.13E-06	* 22	11	3.33E-04	* 13	9	2.44E-05	* 13	27	0.014363	9	22	3.17E-03	* 11	13	8.66E-04	* 10
Other types of O-glycan biosynthesis	47	15	7.66E-06	* 11	82	NS	2	70	NS	2	4	2.08E-06	* 9	14	3.7E-05	* 8	106	NS	1
Cholesterol metabolism	50	16	1.45E-05	* 11	9	6.51E-05	* 8	8	1.01E-05	* 8	55	NS	3	10	7.5E-06	* 9	10	4.24E-04	* 6
Protein export	23	18	5.81E-05	* 7	27	0.02503	3	46	NS	2	10	2.22E-04	* 5	18	3.39E-04	* 5	21	9.96E-03	3
Bile secretion	89	26	2.57E-04	* 13	48	NS	5	37	0.04397	5	17	1.86E-03	* 8	9	6.23E-06	* 12	55	NS	3
Coronavirus disease	232	42	0.02348	18	16	2.21E-03	* 15	55	NS	8	48	NS	10	35	0.026725	12	9	5.9E-05	* 15
Ribosome	158	52	NS	11	4	5.2E-10	* 22	25	7.07E-03	9	196	NS	2	46	NS	8	5	3.18E-10	* 19

B eIF3e^{KD} unique upregulated DTEGs

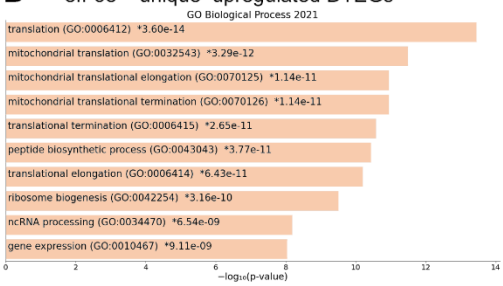

C

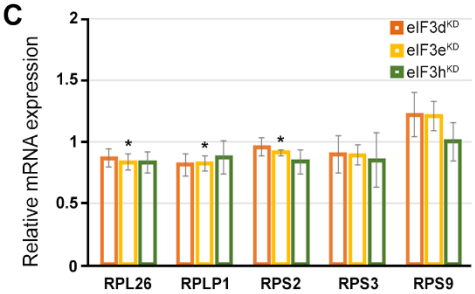

Supplementary Figure 5. **KEGG pathway enrichment analysis of the eIF3d^{KD}- and eIF3e^{KD}-associated upregulated DTEGs reveals upregulation of ribosomal proteins.** **(A)** List of top 10 significantly enriched KEGG pathways for eIF3d^{KD} "all", eIF3e^{KD} "all", eIF3d^{KD}/eIF3e^{KD} "common", eIF3d^{KD} "unique", eIF3d^{KD} "translation only", and eIF3e^{KD} "translation only" groups of upregulated DTEGs. Ranking corresponds to the lowest-to-highest p-value (calculated by Enrichr gene set search engine), with the "eIF3d^{KD} all" group setting the primary ranking. Less significant terms ranking 11 and below are in grey. Terms specifically discussed in the main text are highlighted in green. For each term, the total number of genes in the pathway and number of DTEGs found in each pathway is indicated. Only significant p-values (< 0.05) are shown. NS = not significant p-value (> 0.05) Asterisk next to a p-value indicates that a given term also has a significant Benjamini-Hochberg adjusted p-value (< 0.05). **(B)** The bar chart shows the top 10 enriched GO Biological Process terms for eIF3e^{KD} "unique upregulated" DTEGs, along with their corresponding p-values. **(C)** Relative mRNA expression of selected Ribosomal protein genes normalized to NT control = 1. One-sample t-test was used for statistical evaluation, * = P<0.05.

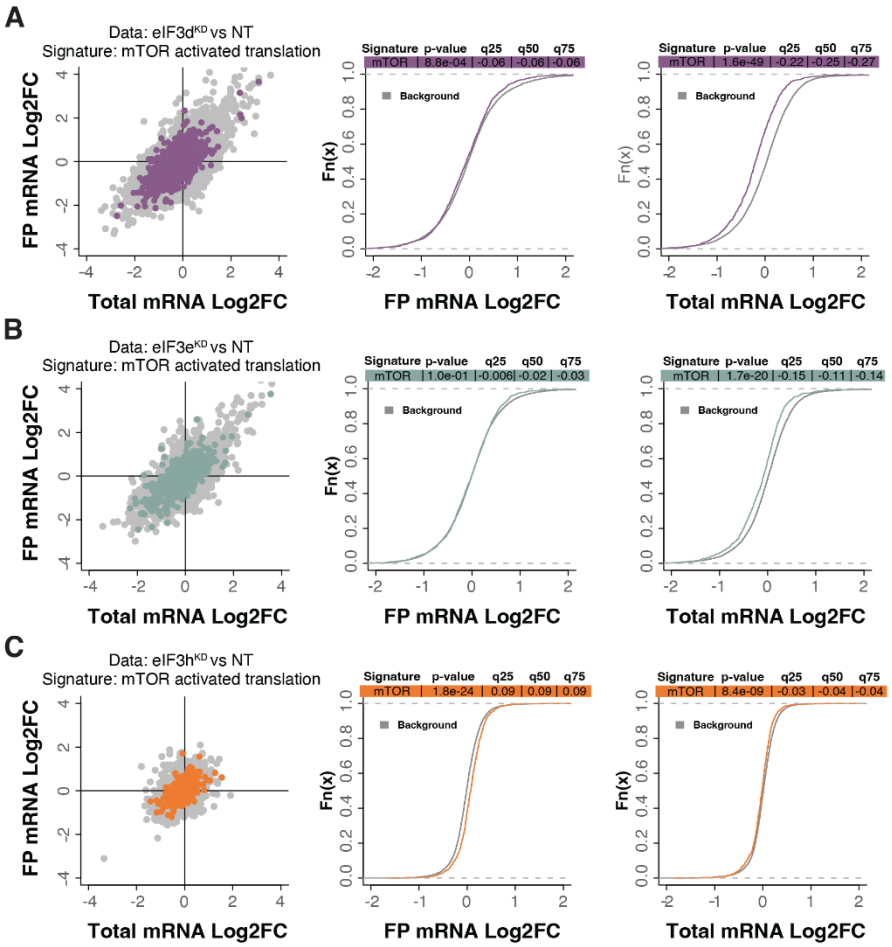

Supplementary Figure 6. **mTOR-sensitive transcripts are translationally offset (buffered) with loss of eIF3d and eIF3e. (A-C)** Scatterplots from translatome analysis of eIF3d^{KD} **(A)**, eIF3e^{KD} **(B)**, and eIF3h^{KD} **(C)** with the location of transcripts that are translationally activated by insulin stimulation (mTOR activation) (Gandin et al., 2016) colored (left panels). Middle and right panels show the empirical cumulative distribution functions of $\log_2$ fold changes in FP and total mRNA for the transcripts that are translationally activated by mTOR signaling. The background constituting all other transcripts are shown as grey curves. Significant differences between the distributions were identified using the Wilcoxon rank-sum test. Differences between the distributions at each quantile are indicated.

A

		eIF3dKD all downregulated			eIF3eKD all downregulated			eIF3dKD/eIF3eKD common downregulated		
KEGG term	**# of genes in pathway**	**rank**	**p-value**	**# of genes**	**rank**	**p-value**	**# of genes**	**rank**	**p-value**	**# of genes**
Chronic myeloid leukemia	76	1	1.652E-10	21	10	7.793E-08	14	7	4.321E-09	14
Neurotrophin signaling pathway	119	2	3.414E-10	26	2	4.614E-09	19	9	5.603E-09	17
Autophagy	141	3	3.734E-10	29	1	1.538E-09	21	2	1.183E-09	19
MAPK signaling pathway	294	4	2.572E-09	42	5	1.221E-08	30	12	2.115E-08	26
Yersinia infection	137	5	8.208E-09	26	4	8.945E-09	20	3	1.183E-09	19
Oocyte meiosis	131	6	1.017E-08	25	11	1.004E-07	18	11	1.941E-08	17
Ubiquitin mediated proteolysis	142	7	1.316E-08	26	9	7.000E-08	19	10	1.103E-08	18
Dopaminergic synapse	132	8	1.654E-08	25	3	4.637E-09	20	1	6.206E-10	19
Fc gamma R-mediated phagocytosis	97	9	2.002E-08	21	7	4.742E-08	16	4	1.845E-09	16
Renal cell carcinoma	69	10	5.914E-08	17	14	1.722E-07	13	18	1.085E-07	12
Human cytomegalovirus infection	225	11	6.852E-08	33	6	3.805E-08	25	5	1.899E-09	24
T cell receptor signaling pathway	104	14	3.406E-07	20	13	1.298E-07	16	8	5.269E-09	16
Shigellosis	247	20	1.661E-06	33	8	5.666E-08	26	6	2.391E-09	25

B

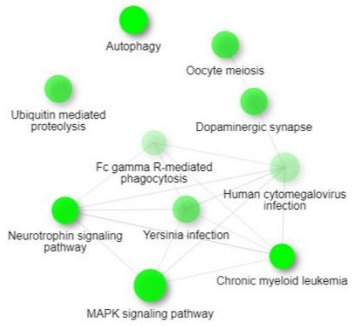

C

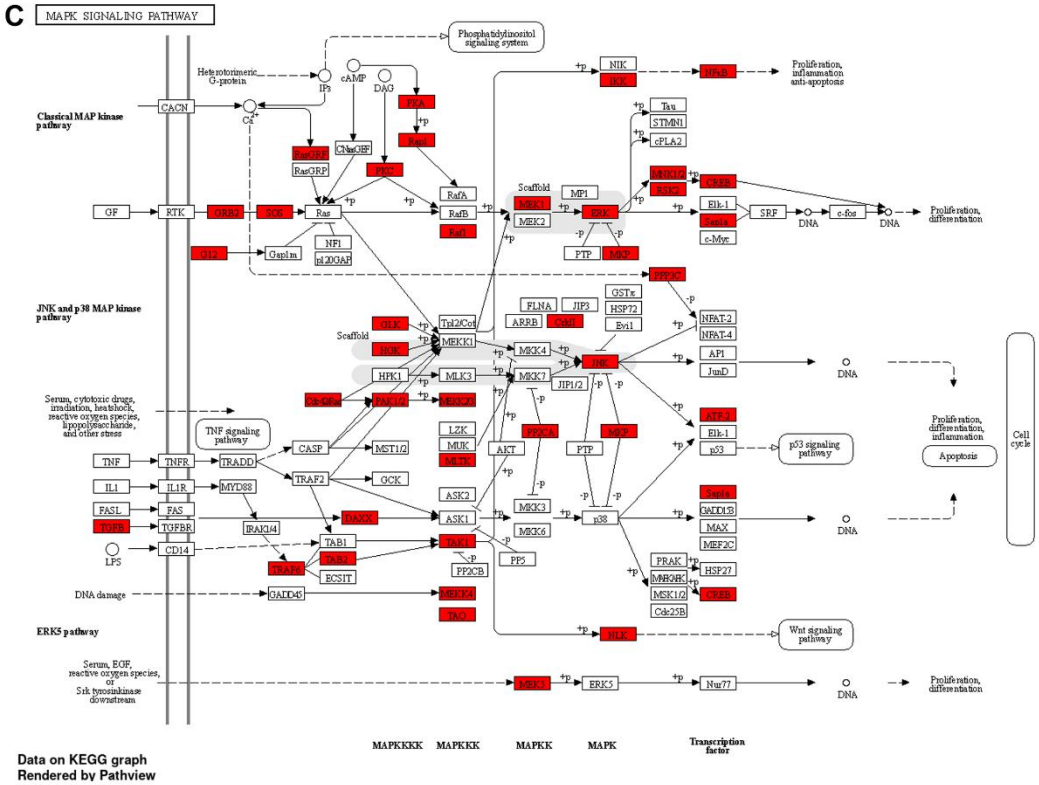

Data on KEGG graph
Rendered by Pathview

Supplementary Figure 7. **KEGG pathway enrichment analysis of the eIF3d^{KD}- and eIF3e^{KD}-associated downregulated DTEGs reveals downregulation of MAPK signaling pathway components. (A)** List of top 10 significantly enriched KEGG pathways for eIF3d^{KD} “all”, eIF3e^{KD} “all”, and eIF3d^{KD}/eIF3e^{KD} “common” groups of downregulated DTEGs. Ranking corresponds to the lowest-to-highest p-value (calculated by Enrichr gene set search engine), with the “eIF3d^{KD} all” group setting the primary ranking. Less significant terms ranking 11 and below are in grey. For each term, the total number of genes in the pathway and number of DTEGs found in each pathway is indicated. All results presented have also significant adjusted p-values as calculated using the Benjamini-Hochberg (BH) procedure to account for multiple hypotheses. **(B)** Network graph of the top 10 most significantly enriched KEGG terms for the eIF3d^{KD} “all downregulated” group of DTEGs. Related KEGG terms are connected with a solid line if they share 20% or more genes. Darker nodes represent more significantly enriched gene sets. Greater nodes represent larger gene sets. **(C)** The KEGG MAPK signaling pathway hsa04010 scheme. Downregulated DTEGs in eIF3d^{KD} matching the genes of this pathway are highlighted in red. See text and Supplementary Spreadsheet S2 for further details.

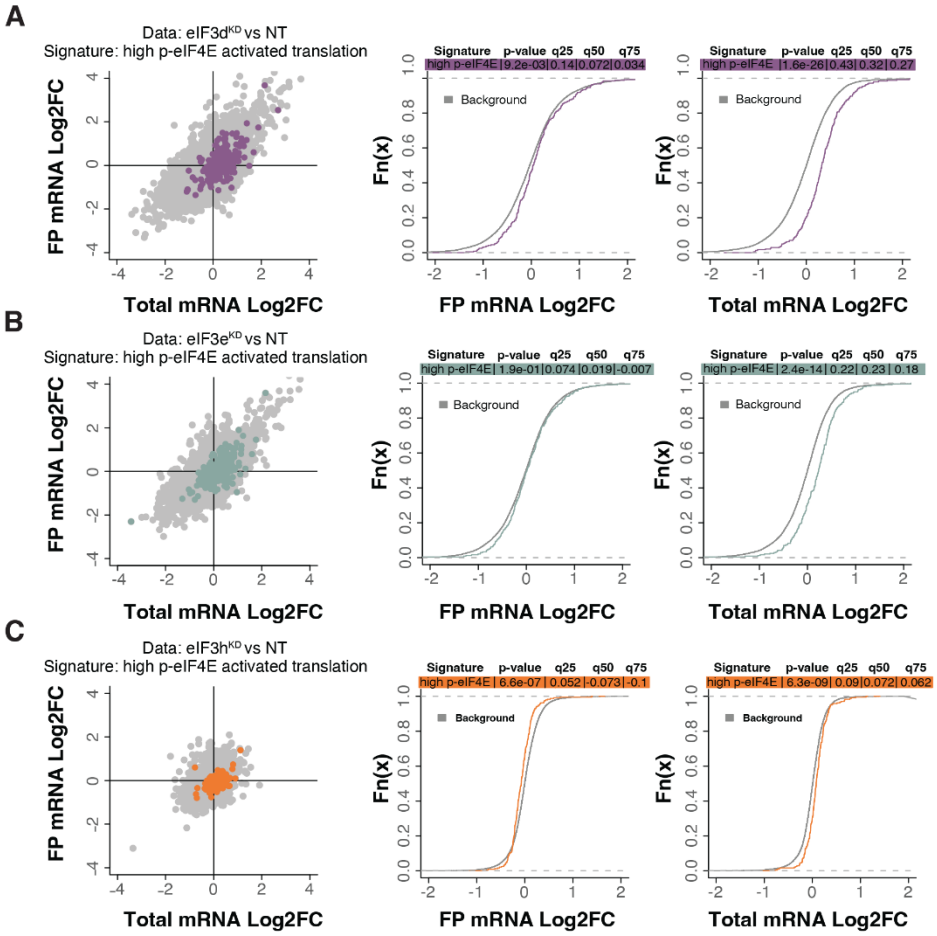

Supplementary Figure 8. **Loss of eIF3 subunits leads to translational offsetting of transcripts with enhanced translation downstream of phosphorylated eIF4E. (A-C)** Scatterplots from translatome analysis of eIF3d^{KD} **(A)**, eIF3e^{KD} **(B)**, and eIF3h^{KD} **(C)** with the location of transcripts translationally activated by high phosphorylation of eIF4E (Karampelias et al., 2022) colored (left panels). Middle and right panels show the empirical cumulative distribution functions of $\log_2$ fold changes in FP and total mRNA for the p-eIF4E sensitive transcripts. The background constituting all other transcripts are shown as grey curves. Significant differences between the distributions were identified using the Wilcoxon rank-sum test. Differences between the distributions at each quantile are indicated.

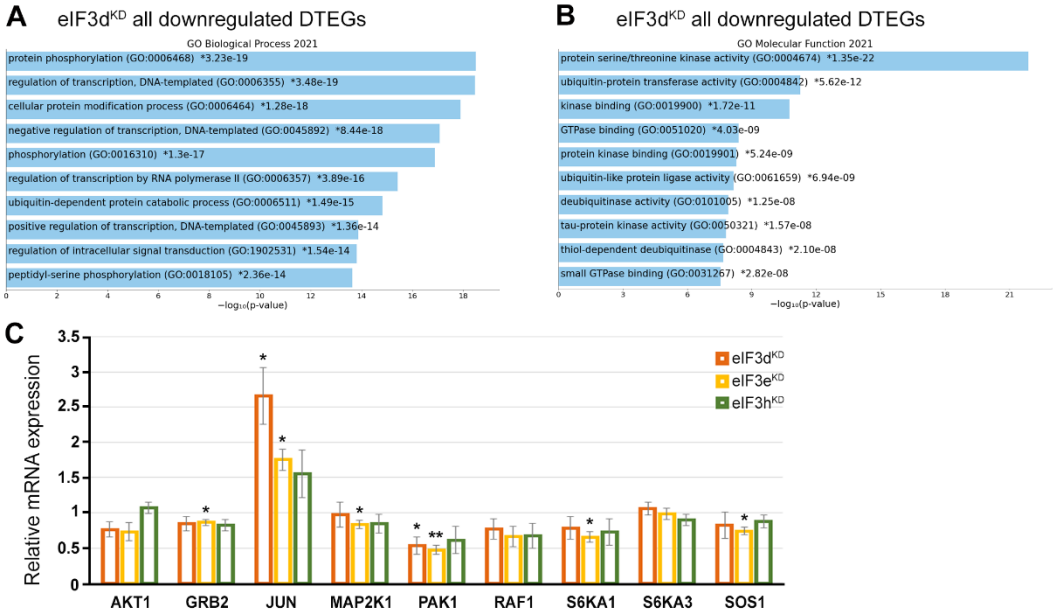

Supplementary Figure 9. **GO enrichment analysis for eIF3d^{KD} associated downregulated DTEGs. (A)** The bar chart shows the top 10 enriched GO Biological Process terms for eIF3d^{KD} "all downregulated" DTEGs, along with their corresponding p-values. **(B)** The bar chart shows the top 10 enriched GO Molecular Function terms for eIF3d^{KD} "all downregulated" DTEGs, along with their corresponding p-values. **(A-B)** Colored bars correspond to terms with significant p-values (<0.05). Asterisk indicates that a given term also has a significant adjusted p-value (<0.05). All P-values were calculated by Enrichr gene set search engine. **(C)** Relative mRNA expression of selected genes from MAPK signaling pathway normalized to NT control = 1. One-sample t-test was used for statistical evaluation, P-values: * = P<0.05, ** = P<0.01.

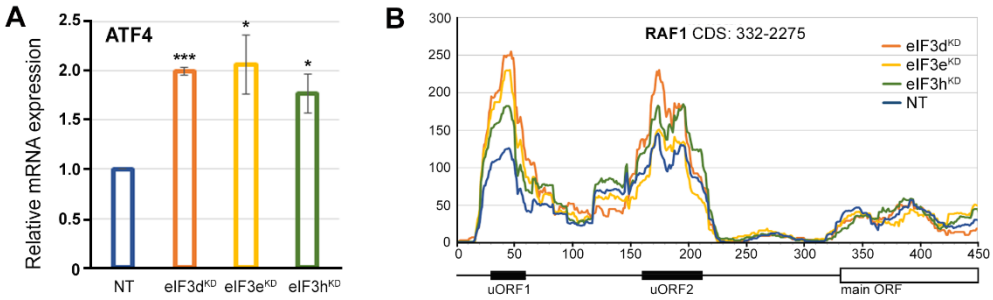

Supplementary Figure 10. **The *ATF4* mRNA is transcriptionally upregulated in all three eIF3 knock-downs tested. (A)** Relative mRNA expression of ATF4 transcription factor, One-sample t-test was used for statistical evaluation, * = P<0.05, *** = P<0.001. **(B)** Normalized ribosomal footprint coverage along the *RAF1* mRNA (first 450 nucleotides). Schematic with regulatory elements is shown at the bottom. Average of all three replicates is shown. Footprint coverage was normalized to all footprints mapping to *RAF1* mRNA.

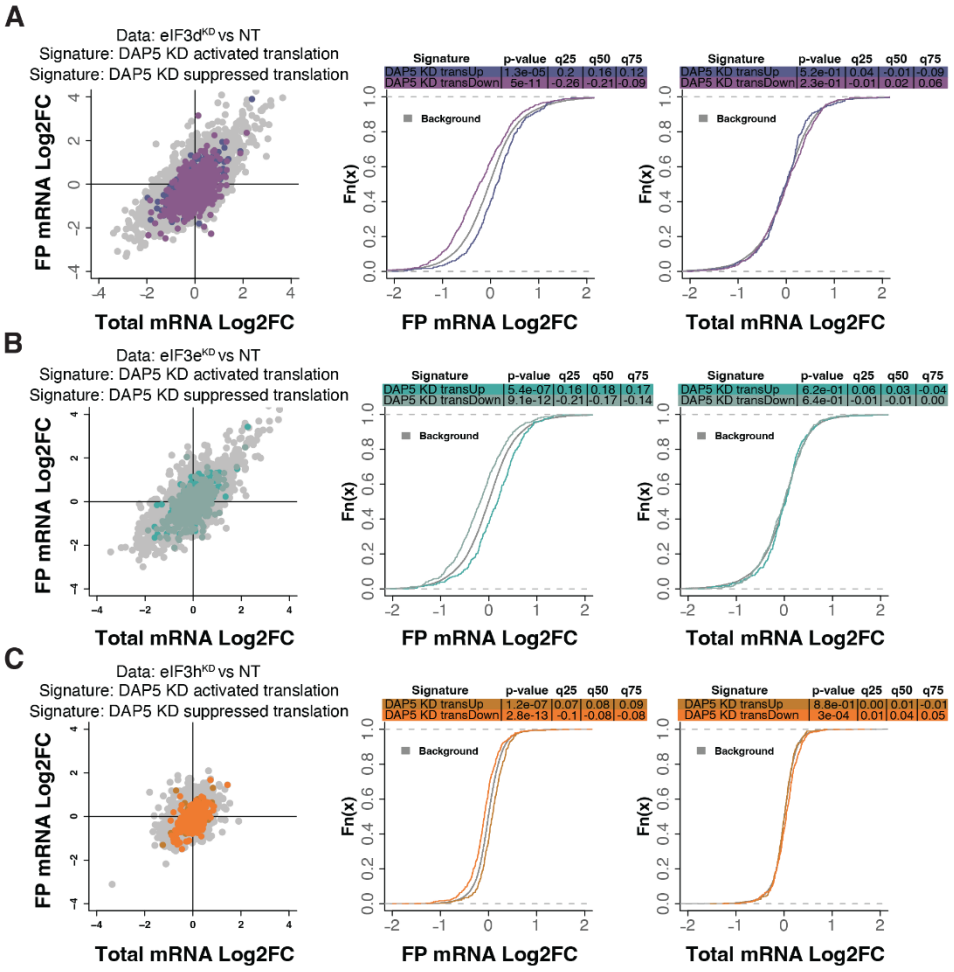

Supplementary Figure 11. **Loss of eIF3 subunits modulates signatures of DAP5-dependent translation. (A-C)** Scatterplots from translatome analysis of eIF3d^{KD} **(A)**, eIF3e^{KD} **(B)**, and eIF3h^{KD} **(C)** with the location of transcripts that are translationally activated and suppressed by KD of DAP5 (David et al., 2022) colored (left panels). Middle and right panels show the empirical cumulative distribution functions of $\log_2$ fold changes in FP and total mRNA for the transcripts that are translationally activated or suppressed upon loss of DAP5. The background constituting all other transcripts are shown as grey curves. Significant differences between the distributions were identified using the Wilcoxon rank-sum test. Differences between the distributions at each quantile are indicated.

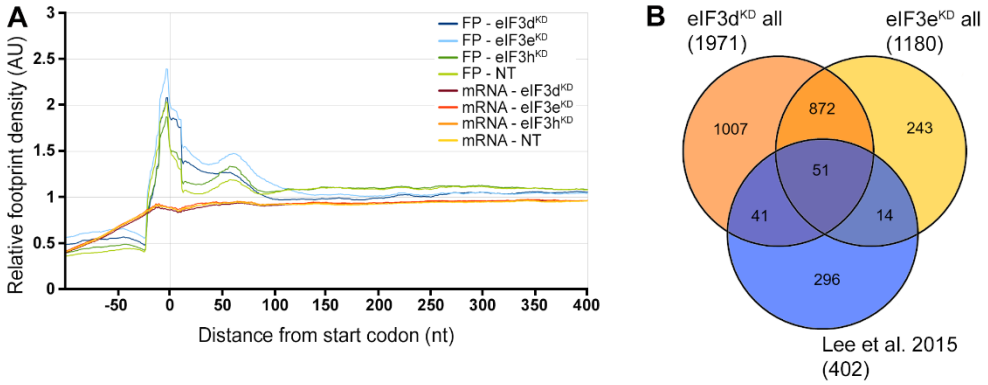

Supplementary Figure 12. **eIF3d^{KD}, eIF3e^{KD}, and eIF3h^{KD} do not show accumulation of footprints at the beginning of CDSes, as reported previously, but display a significant overlap with mRNAs directly interacting with eIF3. (A)** Metagene plot of ribosome density distribution around the start codon of all mRNAs in eIF3d^{KD}, eIF3e^{KD} and eIF3h^{KD}. The plot shows averages of triplicates from Ribo-Seq and quadruplicates from RNA-Seq. **(B)** Venn diagram of the overlap between eIF3d/e^{KD} DTEGs and mRNAs directly interacting with eIF3 as determined by the CLIP assay in (Lee et al., 2015).

Supplementary Table S1. siRNAs used in the study.

ON-TARGETplus siRNA DHARMACON	cat #
eIF3d	L-017556-00
eIF3e	L-010518-00
eIF3h	L-003883-00
Non-targeting	D-001810-03

Supplementary Table S2. qPCR primers used in the study.

Name	5ˈto 3ˈ sequence
Akt1*	CTTCTTTGCCGGTATCGTG
Akt1-R*	TGCTGTCATCTTGGTCAGG
ALAS1	CCACTGGAAGAGCTGTGTGATGTG
ALAS1-R	GCGATGTACCCTCCAACACAACC
ATF4	AAACCTTACGATCCTCCTGGAG
ATF4-R	TGGCTGCTGTCTTGTTTTGC
eIF3b*	TGTGAAAGGTACCTGGTGAC
eIF3b R*	AATAGGCCAATGGGCTGAG
eIF3d	CCAACCCAAACCCGTTTGTG
eIF3d R	TCTTCAGCTCCGTGGCAATG
eIF3e	CTGGTTCCAGCAACAGATAG
eIF3e R	GTGGCTGATAAAGGAAGAGG
eIF3h*	GCTGACTTTGATGAAGTCCA
eIF3h R*	ATGTGGACTGATACCAGCC
GRB2*	CTCTGTCAAGTTTGGAAACGA
GRB-R*	TGAACTTCACCACCCAGAG
Jun*	CAACATGCTCAGGGAACAG
Jun-R*	ACTGTTAACGTGGTTCATGAC
MAP2K1*	CCAGAAAGCTAATTCATCTGGAG
MAP2K1-R*	GTTGCACTCATGCAGAACC
PAK1*	CTTTGACCCGGAATACTGAG
PAK1-R*	CACTATGCTTCGTAATTTCTCC
RAF1*	CACAACTTTGCTCGGAAGAC
RAF1-R*	ACATCGAAATCCATTGAGCAG
RPL26*	GATGATGAAGTTCAGGTTGTACG
RPL26-R*	CATATTTCTTCCTGTAAACCTGGAC
RPLP1*	CTACTCGGCCCTCATTCTG
RPLP1-R*	CCACTTTCTTCTCCTCAGC
RPS2*	AGATCATTGATTTCTTCCTGGG

RPS2-R*	CAACAAATGCCTTGAACCTG
RPS3*	TTATCTTAGCCACCAGAACAC
RPS3-R*	TCTTCTGAACTACAGCAGTC
RPS6KA1*	AACGCTGAAAGTACGTGAC
RPS6KA1-R	CATAGTGCAGCTTCACCAC
RPS6KA3*	CTATACAATGCTTACCGGTTACAC
RPS6KA3-R*	CTACCTATTCGTGCCAATATTTCC
RPS9*	AAGAGCTGAAGCTGATCGG
RPS9-R*	AATTTGACCCTCCAGACCTC
SOS1*	TGGTGTCCTTGAGGTTGTC
SOS1-R*	GGCGACTTGGTATTTGCTC

*primers' sequences were obtained from the database GETPrime, available at http://bbcftools.epfl.ch/getprime

Supplementary Table S3. Antibodies used in the study.

Antibody	source
AKT1	Cell Signaling # 2938
ATF4	Cell Signaling # 11815
eIF3b	Thermo Scientific # PA5-23278
eIF3d	Sigma # HPA066216
eIF3e	Thermo Scientific # PA5-29487
eIF3h	Cell Signalling # 3413
ERK1/2	Santa Cruz # sc-514302
P-ERK1/2	Cell Signaling # 4370
GAPDH	ThermoScientific # PA1-987
GRB2	BD Transduction Laboratories # 610112
JUN	Cell Signaling # 9165
P-JUN	Cell Signaling # 9261
MDM2	Cell Signaling # 86934
MEK1	BD Transduction Laboratories # 610122
PAK1	Santa Cruz # sc-881
RAF	Santa Cruz # sc-133
RPL13A	Cell Signaling # 2765
RPL26	Cell Signaling # 5400
RPLP1	Sigma # HPA003368
RPS2	Santa Cruz # sc-130399
RPS3	Proteintech # 15198-1-AP
RPS9	Thermo Scientific # PA5-13569
RSK1	Santa Cruz # sc-231

RSK2	Santa Cruz # sc-9986
SOS1	Cell Signaling # 12409

Supplementary Table S4. eIF3h^{KD} "all downregulated" DTEGs, top 8 significant results from KEGG pathways as evaluated by Enrichr.

Term	p-value	Overlap genes
Prostate cancer	0.003773	MDM2, ATF4
Aldosterone synthesis and secretion	0.003849	PRKD3, ATF4
Viral carcinogenesis	0.015649	MDM2, ATF4
Human cytomegalovirus infection	0.018997	MDM2, ATF4
Endocytosis	0.023483	MDM2, RAB11FIP2
Bladder cancer	0.038256	MDM2
PI3K-Akt signaling pathway	0.043814	MDM2, ATF4
Cocaine addiction	0.045558	ATF4

Supplementary Table S5. eIF3h^{KD} "all downregulated" DTEGs, top 10 significant results from GO Biological Process as evaluated by Enrichr.

Term	p-value	Overlap genes
Protein ubiquitination	0.001329	RNF10, RMND5A, WAC, MDM2
Mitotic G1 DNA damage checkpoint signaling	0.001716	WAC, MDM2
Protein autoubiquitination	0.001716	RNF10, MDM2
Protein deubiquitination	0.001946	ZRANB1, USP38, MDM2
Protein modification by small protein removal	0.002139	ZRANB1, USP38, MDM2
Proteolysis involved in cellular protein catabolic process	0.002217	ZRANB1, MDM2
RNA splicing	0.003849	IVNS1ABP, SNRPG
Regulation of proteasomal ubiquitin-dependent protein catabolic process	0.004162	WAC, MDM2
Ubiquitin-dependent protein catabolic process	0.004316	ZRANB1, RMND5A, MDM2
Protein K29-linked deubiquitination	0.004741	ZRANB1

Supplementary References

Chothani, S., Adami, E., Ouyang, J.F., Viswanathan, S., Hubner, N., Cook, S.A., Schafer, S., and Rackham, O.J.L. (2019). deltaTE: Detection of Translationally Regulated Genes by Integrative Analysis of Ribo-seq and RNA-seq Data. Curr Protoc Mol Biol *129*, e108.

David, M., Olender, T., Mizrahi, O., Weingarten-Gabbay, S., Friedlander, G., Meril, S., Goldberg, N., Savidor, A., Levin, Y., Salomon, V.*, et al.* (2022). DAP5 drives translation of specific mRNA targets with upstream ORFs in human embryonic stem cells. RNA *28*, 1325-1336.

Durinck, S., Spellman, P.T., Birney, E., and Huber, W. (2009). Mapping identifiers for the integration of genomic datasets with the R/Bioconductor package biomaRt. Nat Protoc *4*, 1184-1191.
Gandin, V., Masvidal, L., Cargnello, M., Gyenis, L., McLaughlan, S., Cai, Y., Tenkerian, C., Morita, M., Balanathan, P., Jean-Jean, O.*, et al.* (2016). mTORC1 and CK2 coordinate ternary and eIF4F complex assembly. Nat Commun *7*, 11127.
Karampelias, C., Watt, K., Mattsson, C.L., Ruiz, A.F., Rezanejad, H., Mi, J., Liu, X., Chu, L., Locasale, J.W., Korbutt, G.S.*, et al.* (2022). MNK2 deficiency potentiates beta-cell regeneration via translational regulation. Nat Chem Biol *18*, 942-953.
Lauria, F., Tebaldi, T., Bernabo, P., Groen, E.J.N., Gillingwater, T.H., and Viero, G. (2018). riboWaltz: Optimization of ribosome P-site positioning in ribosome profiling data. PLoS Comput Biol *14*, e1006169.
Lee, A.S., Kranzusch, P.J., and Cate, J.H. (2015). eIF3 targets cell-proliferation messenger RNAs for translational activation or repression. Nature *522*, 111-114.
Love, M.I., Huber, W., and Anders, S. (2014). Moderated estimation of fold change and dispersion for RNA-seq data with DESeq2. Genome Biol *15*, 550.
Wagner, S., Herrmannova, A., Sikrova, D., and Valasek, L.S. (2016). Human eIF3b and eIF3a serve as the nucleation core for the assembly of eIF3 into two interconnected modules: the yeast-like core and the octamer. Nucleic Acids Res *44*, 10772-10788.